ORIGINAL ARTICLE

Coupling between the spin precession and polar motion of a synchronously rotating satellite: application to Titan

Rose-Marie Baland[1] · Alexis Coyette[2] · Tim Van Hoolst[1]

Abstract

We here develop, in an angular momentum approach, a consistent model that integrates all rotation variables and considers forcing both by the central planet and a potential atmosphere. Existing angular momentum approaches for studying the polar motion, precession, and libration of synchronously rotating satellites, with or without an internal global fluid layer (e.g., a subsurface ocean) usually focus on one aspect of rotation and neglect coupling with the other rotation phenomena. The model variables chosen correspond most naturally with the free modes, although they differ from those of Earth rotation studies, and facilitate a comparison with existing decoupled rotation models that break the link between the rotation motions. The decoupled models perform well in reproducing the free modes, except for the Free Ocean Nutation in the decoupled polar motion model. We also demonstrate the high accuracy of the analytical forced solutions of decoupled models, which are easier to use to interpret observations from past and future space missions. We show that the effective decoupling between the polar motion and precession implies that the spin precession and its associated mean obliquity are mainly governed by the external gravitational torque by the parent planet, whereas the polar motion of the solid layers is mainly governed by the angular momentum exchanges between the atmosphere (e.g., for Titan) and the surface. To put into perspective the difference between rotation models for a synchronously rotating icy moon with a thin ice shell and classical Earth rotation models, we also consider the case of the Moon, which has a thick outer layer above a liquid core. We also show that for non-synchronous rotators, the free precession of the outer layer in space degenerates into the tilt-over mode.

Keywords Cassini state · Precession · Polar motion · Titan · Internal ocean · Angular momentum formalism

1 Introduction

Synchronous rotation is a common phenomenon in our Solar system. Be it the Moon, the Galilean satellites, or Titan, almost every large satellite of the planets of the Solar system has

✉ Rose-Marie Baland
rose-marie.baland@oma.be

1 Royal Observatory of Belgium, Ringlaan 3, 1180 Brussels, Belgium

2 UNamur, Namur Institute for Complex System (naXys), Namur, Belgium

equal rotation and revolution periods. This is a consequence of the dissipation associated with the tides raised by the parent planet on the satellite which tends to slow down the satellite's rotation. Such synchronous rotators are expected to occupy a Cassini state, which is a special equilibrium configuration described at the end of the seventeenth century by Cassini for the Moon (see Colombo 1966, for a modern description). In that state, the precession of the rotation axis is driven by the precession of the orbit pole, so that the nodes of the orbital plane and of the equatorial plane are locked together, and that the spin axis lies in the plane defined by the orbit and Laplace poles, whereas the obliquity remains constant. The Laplace plane is the inertial plane that minimizes the variations in orbital inclination and can be seen as an orbital plane averaged over the node precession period. The obliquity is the angular separation between the orbit pole and the spin axis. While the spin axis precesses in space, it wobbles with respect to the rotating frame attached to the surface of the satellite. This motion is called polar motion.

Unlike polar motion, the spin precession has been observed for Titan and the Moon. The orientation of the spin axis of the mantle of the Moon has been determined from Lunar laser ranging (see Williams et al. 2001 and references therein). The inclinations of the orbit and of the equator of the Moon with respect to the ecliptic are $i = 5.145°$ and $\theta = -1.543°$, respectively. Both planes precess retrogradely with a period of 18.6 years. The obliquity $\varepsilon = \theta - i = -6.688°$ is consistent with the obliquity of an entirely solid and rigid Moon [$\simeq -6.8°$, as can be obtained, e.g., from Eq. (6) of Baland et al. (2011)]. Recently, Dumberry and Wieczorek (2016) studied the orientation of the inner core, in view of a possible validation of dynamo models and detection in gravity signal of a differential orientation of the inner core with respect to the mantle. Titan is the only satellite of the Solar system with a significant atmosphere, which is expected to be the main cause of the polar motion of satellite (Coyette et al. 2016, 2018). The orientation of the spin axis of the shell of Titan has been determined from Cassini radar images (see Meriggiola et al. 2016 and references therein). The obliquity $\varepsilon = 0.31°$ whereas the orbital inclination with respect to the Laplace plane $i = 0.32°$ and the period of the retrograde precession is about 700 years. The obliquity is about three times larger than expected for an entirely solid and rigid Titan. Bills and Nimmo (2008) proposed that the presence of a subsurface ocean can explain Titan's large obliquity. It is currently believed that the large obliquity of Titan is due to a resonant amplification, allowed by the presence of the internal ocean (Baland et al. 2011; Noyelles and Nimmo 2014; Boué et al. 2017).

The rotation models mentioned above have some drawbacks. In polar motion models (Coyette et al. 2016, 2018), the spin precession is set as known and not solved for, whereas the polar motion is set to zero in the spin precession model of Baland et al. (2011). We refer to that kind of models as decoupled models in the following. Contrary to decoupled polar motion model of Coyette et al. (2018), the decoupled spin precession model of Baland et al. (2011) does not include the possibility of a thick atmosphere/lakes exchanging angular momentum with the surface and does not include ocean flow. The effects of an ocean flow and an atmosphere are also not considered in the model of Noyelles and Nimmo (2014), which couples the spin precession to polar motion. The model of Dumberry and Wieczorek (2016) for the Moon includes precession/polar motion coupling and the flow in the liquid core, but is not suited for a study of the polar motion, as we will see later, whereas the model by Boué et al. (2017) includes precession/polar motion coupling, ocean flow, but not the effect of Titan's atmosphere. Finally, except for Williams et al. (2001) in the case of a solid Moon, and Coyette et al. (2016, 2018) in the case of Titan with an ocean, the effect of periodic tidal deformations is not considered in the aforementioned studies (see Baland et al. 2016 for an update of Baland et al. (2011) to tidal deformations, or Noyelles (2018) for a coupled rotation model of a tidally deformed solid body).

In this study, we investigate all rotation variations (libration, precession, polar motion) in one consistent model that integrates the effects of the existence of internal (e.g., subsurface ocean) and external (atmosphere) non-solid layers. We use the angular momentum formalism and focus on the spin precession and the polar motion and their coupling to each other. Since decoupled models offer the advantage of providing compact analytical solutions, we also assess their validity.

The plan of the paper is as follows. In Sect. 2, in order to study the coupling between polar motion and spin precession in a simple configuration first, we extend the Cassini state model of Eckhardt (1981), originally developed for a solid and rigid Moon, to a solid and rigid Titan and its thick atmosphere. We consider two torques to be applied on the satellite: the quasi-diurnal external gravitational torque by the parent planet and the atmospheric torque, which includes a constant term, and a series of periodic terms. As the atmospheric variations are governed by the revolution of Saturn around the Sun, we mainly focus on the annual term (annual refers to the revolution period of Saturn around the Sun which is 29.42 years). The external torque is said to be quasi-diurnal because its period is slightly altered by the orbital precession period (diurnal refers to the rotation/revolution period of Titan which is 15.9 days). In Sect. 3, we move on to the case with a rotating global internal liquid layer, still considering the precession/polar motion coupling and the atmosphere. We express the different torques as functions of the chosen variables to be solved for. The external gravitational torque on each layer is easily generalized from its expression in the solid case, and the internal gravitational torques are adapted from Coyette et al. (2016). The atmospheric torque exerted on the shell is identical to the atmospheric torque exerted on the solid satellite. We model the flow in the ocean as a simple solid rotation, or Poincaré flow and adopt the procedure of Mathews et al. (1991) for the computation of the total torque exerted on the liquid layer (which turns out to be only caused by the hydrodynamical part of the pressure at the liquid layer boundaries). From the ocean torque, we deduce the hydrodynamic torques on the shell and on the interior. All the torques are introduced in a set of governing equations for the coupled polar motion and spin precession. Neglecting the polar motion of the solid layers and the atmospheric torque, we also write a set of governing equations for the decoupled spin precession, to be used for comparisons with the coupled model instead of the ocean model of Baland et al. (2011) who considered that the ocean is in hydrostatic equilibrium. We show that decoupled models for the polar motion and the spin precession can be very good approximations of the coupled model, and can therefore be used in view of data interpretation. Throughout Sects. 2 and 3, we put into perspectives some differences between the rotation of a synchronous satellite and Earth rotation. We present a summary and concluding remarks in Sect. 4.

2 Entirely solid and rigid satellite

2.1 Governing equations

We first consider the case of an entirely solid and rigid satellite in order to be able to later assess the effect of a subsurface ocean on the satellite's rotation. An additional advantage is that the mathematics of a solid satellite is less complex, which allows us to focus here on more geometrical aspects and facilitates comparisons with previous results. This will also allow putting into perspective the differences between synchronous and non-synchronous rigid rotation (e.g., the rotation of a rigid Earth, which is a very well-known problem).

The rotation variations of a solid synchronous body locked in the Cassini state is a problem that can be divided into three components:

1. The variations in rotation angle. We will refer to them as **librations** when they are caused by the external gravitational torque by the parent body and as **LOD variations** when they are caused by exchanges of angular momentum between the outer solid layer and the atmosphere and/or lakes present on the surface, e.g., for Titan,
2. The **polar motion**, which is the motion of the rotation axis with respect to the Body Frame (**BF**), a frame attached to the mean principal axes of inertia of the satellite,
3. The motion of the BF with respect to the inertial frame (**IF**), or conversely the motion of the Laplace pole as seen from the BF (**Laplace pole motion** hereafter).

By combining the Laplace pole motion and the polar motion, it is possible to obtain the motion of the rotation axis with respect to the inertial space (see Appendix 1), decomposed in a main motion called **precession**, and smaller motions called **nutations**. The **obliquity** is the angular separation between the normal to the orbit and the spin axis. Even though the precession of the rotation axis with respect to an inertial/Laplace reference frame is likely a more intuitive concept than the Laplace pole motion in the BF, the latter is a more practical component to be solved for when the governing equations are written in the BF, as will be done in this paper.

Often, the equations governing the rotation of a synchronous rigid satellite are solved in an approximated way. For example, Van Hoolst et al. (2013) studies libration and LOD variations without considering polar motion and precession, Bills and Nimmo (2008) and Baland et al. (2011) determine the precession and obliquity from the angular momentum equation written in the IF by neglecting polar motion and librations/LOD variations, whereas Coyette et al. (2016) determine the polar motion from the angular momentum equation written in a rotating BF by considering a coplanar precession with a fixed obliquity whose value can be arbitrarily chosen. The decoupled libration and LOD variations models are accurate since those rotation components are decoupled from the other components (see below). Precession and polar motion, however, are coupled through Euler's kinematic equation (see Eq. 13) and the decoupled models for those rotation components require further justification. Assessing the validity of the decoupled models is one of the goals of this study and is important as they have the advantage of producing rather compact analytical solutions practical for interpretation of measurements (e.g., Margot et al. 2007, 2012 used simple analytical decoupled solutions for both the obliquity and libration of Mercury to infer the polar moment of inertia of its mantle and of its core). We show below that the coupling with polar motion has a small influence on the spin precession: It results in a shift of $\lesssim 0.1\%$ in mean obliquity and even smaller semi-diurnal and diurnal nutations related to the influence of the central planet and of the atmosphere, respectively. We also show that there are very little differences ($\lesssim 0.1\%$) between the results of coupled and decoupled polar motion models.

As proved by Eckhardt (1981), all the components of the rotation of a satellite in synchronous rotation with its orbital motion can be fully described as solutions of a system of two equations written in the BF. The first describes the change in angular momentum and is coupled to the second equation stating that the Laplace pole is fixed in inertial space. We express the rotation vector of the satellite as

$$\mathbf{\Omega} = n \begin{pmatrix} 0 \\ 0 \\ 1 \end{pmatrix} + n \, \mathbf{m} = n \begin{pmatrix} m_x \\ m_y \\ 1 + m_z \end{pmatrix}, \tag{1}$$

with **m** the incremental rotation vector with respect to the synchronous rotation, in which m_x and m_y are the components of the polar motion normalized by n, and m_z represents the normalized variations in rotation rate. The rotation rate n is equal to the mean rate of the satellite's true longitude $L = \Omega + \omega + M$ which is the sum of the ascending orbital node longitude Ω, the pericenter longitude ω, and of the mean anomaly M. We have chosen here the z-axis of the BF along the largest principal moment of inertia. The x-axis points toward the parent body at pericenter and the y-axis is at 90° with respect to the x-axis in such a way that the three axes form a right-handed Cartesian frame.

2.1.1 Angular momentum equation

The angular momentum equation can be expressed in the satellite's BF as

$$\frac{d\mathbf{H}}{dt} + \mathbf{\Omega} \wedge \mathbf{H} = \mathbf{\Gamma}_{\text{pb}} + \mathbf{\Gamma}_{\text{a}} \tag{2}$$

and expresses that the rate of change of the rotation angular momentum

$$\mathbf{H} = \overline{\overline{I}} \mathbf{\Omega} \tag{3}$$

is due to the applied external torques by the parent body ($\mathbf{\Gamma}_{\text{pb}}$) and by the possible atmosphere and lakes which exchange angular momentum with the surface ($\mathbf{\Gamma}_{\text{a}}$). $\overline{\overline{I}}$ is the inertia tensor of the solid and rigid synchronous satellite defined as

$$\overline{\overline{I}} = \begin{pmatrix} A & 0 & 0 \\ 0 & B & 0 \\ 0 & 0 & C \end{pmatrix}, \tag{4}$$

with $A < B < C$ the principal moments of inertia along axes x, y, and z.

External torque: The external torque by the parent body $\mathbf{\Gamma}_{\text{pb}}$ can be written, correct up to first order in small rotational and orbital quantities, as (see Eq. (18) of Coyette et al. (2016) and Appendix 1.2)

$$\mathbf{\Gamma}_{\text{pb}} = 3n^2 \begin{pmatrix} 0 \\ (A - C)[i \sin(\omega + M - \pi) - p_x] \\ (B - A)(s - \gamma) \end{pmatrix}. \tag{5}$$

Here γ is the libration angle ($m_z = \dot{\gamma}/n$) and $s = 2e \sin M$ with e the orbital eccentricity. p_x is the x-component of the unit vector along the Laplace pole expressed with respect to the satellite's BF as

$$\hat{p} = \begin{pmatrix} 0 \\ 0 \\ 1 \end{pmatrix} + \mathbf{p} = \begin{pmatrix} p_x \\ p_y \\ 1 \end{pmatrix}. \tag{6}$$

Since the tilt between the Laplace pole and the BF pole is small, it is a good first-order approximation to set the z-component of $\hat{p}$ to 1 (see Eq. 100). As we intend to derive a coupled solution for polar motion and Laplace pole motion from which we will extract the precession, we have expressed this torque as a function of the *unknown* Laplace pole motion, whereas Coyette et al. (2016) write it as a function of a *known* obliquity and of an *unknown* polar motion. The torque depends on the moment of inertia differences as it would be zero for a spherically symmetric satellite. The z-component depends on $(s - \gamma)$ as this represents the angle between the x-axis and the direction to the planet in the orbital plane. The y-component

depends on the orientation of the equator with respect to the orbital plane expressed here as a function of the orbital inclination i and of the Laplace plane orientation with respect to the BF. Note that the frequency of the first term of the y-component of the external torque is the variation rate of $(M + \omega)$ which is equal to $(n - \dot{\Omega})$ and is quasi-diurnal. *Diurnal* refers to the rotation/revolution period of the synchronous satellite (15.9 days for Titan).

Atmosphere/lakes torque: Titan is the only synchronous satellite which possesses a significant atmosphere, and lakes and seas, that exchange angular momentum with the surface. The details of the derivation of their torque $\mathbf{\Gamma}_a$ on Titan are given in Coyette et al. (2016). They start from the atmospheric angular momentum (AAM) generated from an atmospheric Global Circulation Model for Titan's atmosphere (Tokano 2013), decomposed into time series. Each component of the AAM series is the combination of a pressure/matter term, caused by the time-variable atmospheric pressure on Titan's surface, and of a wind/motion term, caused by the relative motion of the atmosphere with respect to the surface. The angular momentum of the seas and lakes (Tokano et al. 2014; Tokano and Lorenz 2015) is similarly decomposed into series for the pressure and motion terms. In summary, the angular momentum $\mathbf{H}_a$ of the atmosphere and lakes is the sum of a constant term (frequency zero) and of a Fourier series with frequencies ϖ, amplitudes $h_x(\varpi)$, $h_y(\varpi)$, $h_z(\varpi)$, and phases ϕ_x, ϕ_y, ϕ_z:

$$\mathbf{H}_a = \begin{pmatrix} h_x(0) + \sum_{\varpi \neq 0} h_x(\varpi) \cos(\varpi t + \phi_x(\varpi)) \\ h_y(0) + \sum_{\varpi \neq 0} h_y(\varpi) \cos(\varpi t + \phi_y(\varpi)) \\ h_z(0) + \sum_{\varpi \neq 0} h_z(\varpi) \cos(\varpi t + \phi_z(\varpi)) \end{pmatrix}. \tag{7}$$

The angular momentum has an annual component and in addition a multitude of frequencies associated with the atmosphere and lake dynamics. *Annual* refers to the revolution period of Saturn around the Sun (29.42 years). Because of atmospheric super-rotation, $h_z(0)$ dominates all other parts of any components of $\mathbf{H}_a$. At first order in small quantities $m_x, m_y, h_x(\varpi), h_y(\varpi)$ and $h_z(\varpi \neq 0)$, the torque is written as

$$\mathbf{\Gamma}_a = -\frac{\mathrm{d}\mathbf{H}_a}{\mathrm{d}t} - \mathbf{\Omega} \wedge \mathbf{H}_a = \begin{pmatrix} -h_z(0)n m_y + n h_y(0) + \tilde{\Gamma}_x \\ +h_z(0)n m_x - n h_x(0) + \tilde{\Gamma}_y \\ \tilde{\Gamma}_z \end{pmatrix}, \tag{8}$$

$$\tilde{\Gamma}_x = \sum_{\varpi \neq 0} \left(n h_y(\varpi) \cos(\varpi t + \phi_y(\varpi)) + \varpi h_x(\varpi) \sin(\varpi t + \phi_x(\varpi)) \right), \tag{9}$$

$$\tilde{\Gamma}_y = \sum_{\varpi \neq 0} \left(-n h_x(\varpi) \cos(\varpi t + \phi_x(\varpi)) + \varpi h_y(\varpi) \sin(\varpi t + \phi_y(\varpi)) \right), \tag{10}$$

$$\tilde{\Gamma}_z = \sum_{\varpi \neq 0} \varpi h_z(\varpi) \sin(\varpi t + \phi_z(\varpi)). \tag{11}$$

The x and y-components of the torque have a constant term, a term proportional to the polar motion components, and other time-varying terms.

2.1.2 Invariance of the Laplace pole (Euler kinematic equation)

The second equation introduced in Eckhardt (1981) is

$$\frac{\mathrm{d}\hat{p}}{\mathrm{d}t} + \mathbf{\Omega} \wedge \hat{p} = 0 \tag{12}$$

and states that the motion of the Laplace pole $\hat{p}$ with respect to the satellite's BF is not subject to any torque, since the Laplace pole does not move in inertial space. The first two components of Eq. (12) add to the three components of Eq. (2), and allow to solve for the 5 unknowns $(\gamma, m_x, m_y, p_x, p_y)$ describing the libration angle, the orientation of the rotation axis with respect to the BF and the orientation of the Laplace plane with respect to the BF.

If we note $(\tilde{\xi}, \tilde{\theta}, \tilde{\phi})$ the Euler angles[1] between the BF and the IF, and then we can write $\hat{p} = (\sin\tilde{\theta}\sin\tilde{\phi}, \sin\tilde{\theta}\cos\tilde{\phi}, \cos\tilde{\theta})$ and Eq. (12) is equivalent to Euler's kinematic equation (e.g., Van Hoolst 2007; Dehant and Mathews 2015)

$$\dot{\tilde{\theta}} + I\sin\tilde{\theta}\,\dot{\tilde{\xi}} = n(m_x + Im_y)e^{I\tilde{\phi}}, \tag{13}$$

which is a classical relation linking precession of the BF in space and polar motion in the BF.

Assuming that the projection of **p** and **m** on the equatorial plane are circular motions at a common frequency w in the BF (positive for prograde motions, negative for retrograde motions), that is to say that $p_x + Ip_y = pe^{Iwt}$ and $m_x + Im_y = me^{Iwt}$ with p the amplitude of the Laplace pole motion and m the amplitude of the polar motion, it is also possible to write Eq. (12) under the form (e.g., Dumberry and Wieczorek 2016 or Mathews et al. 1991):

$$p = \frac{m}{1 + w/n}. \tag{14}$$

Equations (12–14) do not involve the details of the internal structure of the satellite, hence the adjective *kinematic*.

2.1.3 Final system of governing equations

At first order in small rotational and orbital quantities, the final system of governing equations can be expressed as a system of five ordinary differential equations

$$An\dot{m}_x + [(C-B)n + h_z(0)]nm_y = nh_y(0) + \tilde{\Gamma}_x, \tag{15}$$

$$Bn\dot{m}_y + [(A-C)n - h_z(0)]nm_x = -nh_x(0) + \tilde{\Gamma}_y,$$
$$+3n^2(A-C)[i\sin(\omega + M - \pi) - p_x], \tag{16}$$

$$\dot{p}_x = np_y - nm_y, \tag{17}$$

$$\dot{p}_y = -np_x + nm_x, \tag{18}$$

$$C\ddot{\gamma} + 3n^2(B-A)\gamma = 6en^2(B-A)\sin M + \tilde{\Gamma}_z, \tag{19}$$

in polar motion (m_x, m_y), orientation of the Laplace pole with respect to the BF (p_x, p_y), and libration (γ). Equation (19) governs the libration/LOD variations and is independent of the other equations. We, nevertheless, note that those variations have a negligible effect on the spin precession of the satellite (see Appendix 1). Its solution, which can be written explicitly in analytical form, is well known (e.g., Van Hoolst et al. 2009). We, therefore, focus on the subsystem composed of Eqs. (15–18), which governs the polar motion and the Laplace pole motion, and therefore precession and shows that both motions are coupled. Compared to the system of Eqs. (72–73) of Coyette et al. (2016) for polar motion, two additional equations allow for orientating the BF with respect to the IF. A direct comparison with Eq. (1) of Baland et al. (2011) for the spin precession is not possible, as that equation is written in the

---

[1] Note that the Euler angles $(\tilde{\xi}, \tilde{\theta}, \tilde{\phi})$ of the BF are defined here in the same way as the Euler angles (ξ, θ, ϕ) of the rotation reference frame in Fig. 10. We use a different notation though to avoid confusion.

Table 1 Values for the interior and orbital parameters of a satellite toy model which has the characteristics of Titan, but rotates rigidly

Parameter	Value	References
R	2575 km	Zebker et al. (2009)
$\{A, B, C\}$	$\{3.060104, 3.060465, 3.06058\} \times 10^{35}$ kg m^2	Coyette et al. (2016)
n	$2\pi/15.9$ days	https://ssd.jpl.nasa.gov/?sat_elem
e	0.0288	https://ssd.jpl.nasa.gov/?sat_elem
$\dot{\Omega}$	$-2\pi/703$ years	Vienne and Duriez (1995)
i	$0.3197°$	Vienne and Duriez (1995)
$\{h_x(0), h_y(0), h_z(0)\}$	$\{7 \times 10^{21}, -6 \times 10^{22}, 2.0 \times 10^{26}\}$ kg m^2 s^{-1}	Tokano (2013)
ϖ_{an}	$2\pi/29.42$ years	
$\{h_x(\varpi_{an}), h_y(\varpi_{an})\}$	$\{3.0 \times 10^{22}, 1.0 \times 10^{22}\}$ kg m^2 s^{-1}	Tokano (2013)
$\{\phi_x(\varpi_{an}), \phi_y(\varpi_{an})\}$	$\{0.9, 5.19\}$ rad	Tokano (2013)

The toy satellite has no surface lakes and the atmosphere dynamics has only constant and annual terms. Its orbital precession is taken to be uniform. In some places the toy model is simplified to the axisymmetric case ($A = B$, using the value of $(A + B)/2$)

IF after averaging over the rotation/revolution period and with the assumption of a zero polar motion.[2]

The PM/precession subsystem is characterized by two free modes, obtained by averaging the torques over the forcing periods to get homogeneous equations. One of them is the free polar motion, which by analogy with the Earth is called the **Chandler Wobble** (CW). The other is the free precession (FP) of the spin axis around the Laplace pole. We refer to the latter free mode as the **Quasi-Diurnal Free Wobble** (QDFW) since it has a long period in inertial space but is quasi-diurnal in the BF. In the next subsections, we derive the free frequencies, eigenmodes, and forced solutions of the PM/precession subsystem. We consider for illustrative purposes a satellite toy model with some of Titan's characteristics (see Table 1).

2.2 Free frequencies

The frequencies σ_{CW} and σ_{QDFW} of the free modes have expressions of the form

$$\sigma_{CW} = \sqrt{\frac{Z - \sqrt{\Delta}}{2AB}} \quad \text{and} \quad \sigma_{QDFW} = \sqrt{\frac{Z + \sqrt{\Delta}}{2AB}}, \tag{20}$$

$$Z = n^2 \left[-3A^2 + 2A(B + C) + C(C - B)\right] - h_z(0)n(A + B - 2C) + h_z(0)^2, \tag{21}$$

$$\Delta = Z^2 - 4ABn^2 \left[4(C - A)n + h_z(0)\right]\left[(C - B)n + h_z(0)\right]. \tag{22}$$

At first order in $(C - A)$, $(C - B)$, and $h_z(0)$, which are small quantities with respect to A, B, and C, Eqs. (20–22) simplify to

$$\sigma_{CW} \simeq 2n\sqrt{\frac{(C - B + h_z(0)/n)(C - A + h_z(0)/4n)}{AB}}, \tag{23}$$

$$\sigma_{QDFW} \simeq n + \frac{3}{2}n\frac{C - A}{A}. \tag{24}$$

---

[2] See Appendix A of Baland et al. (2012) for the derivation of Eq. (1) of Baland et al. (2011) from Eqs. (2) and (100), assuming $m_x = m_y = 0$.

Table 2 Period of the Free modes of the Titan toy model (see Table 1), computed from Eqs. (20–22), considering the triaxial or biaxial cases, and the presence or absence of the atmosphere

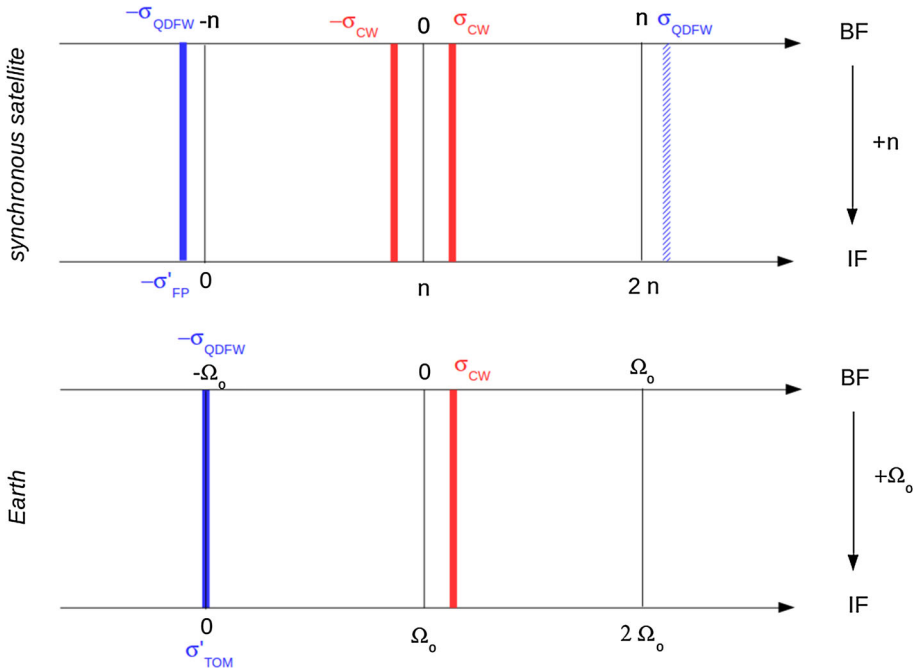|	Triaxial		Biaxial	
	+ Atm.	No Atm.	+ Atm.	No Atm.
T_{CW} (years)	116.36	278.77	121.39	224.44
T_{QDFW} (days)	15.8963	15.8963	15.8977	15.8977
T_{FP} (years)	185.094	185.067	296.631	296.589

Fig. 1 Free frequencies in the BF and in the IF for a triaxial synchronous rotator (top) and for a biaxial non-synchronous rotator (e.g., the Earth, bottom). The passage from the BF to the IF is obtained by adding the rotation rate (n or Ω_o) to the free frequencies expressed in the BF. Positive/negative frequencies correspond to prograde/negative motions. Some remarkable frequencies have received a denomination: Quasi-Diurnal Free Wobble (QDFW), Chandler Wobble (CW), Free Precession (FP), and Tilt-Over mode (TOM). The prograde QDFW has a very small amplitude compared to the retrograde QDFW, hence the hatched line. For a biaxial Earth, the modes are purely prograde (CW) or retrograde (QDFW) in the BF

Whereas the CW is affected by the atmosphere, the QDFW is not affected at first order (see also Table 2 for numerical results for the Titan toy model). Neglecting the effect of the atmosphere super-rotation ($h_z(0) = 0$), Eqs. (23–24) are equivalent to Eqs. (8a–8b) of Eckhardt (1981) [see also Eqs. (41–42) of Varadi et al. (2005) and Sect. 3 of Rambaux and Williams (2011)], and Eqs. (20–22) are equivalent to Eq. (90) derived by Boué et al. (2017) within an Hamiltonian formalism.

We have written the free frequencies as positive, but the system is in fact characterized by two pairs of equal and opposite eigenvalues, related to the fact that each eigenmode is a combination of circular prograde and retrograde motions (see below and Fig. 1). In inertial space, the circular motions of frequency σ translate to motion of frequency $\sigma' = \sigma + n$. In particular, the circular retrograde QDFW translates into a circular retrograde free precession

at rate (written as a positive value)

$$\sigma'_{\text{FP}} = \frac{3}{2} n \frac{C - A}{A}. \tag{25}$$

Like the QDFW, the FP is not significantly affected by the atmosphere. The smaller the difference between C and A is, the larger the free precession period is (see Table 2).

The first-order approximation for the free frequencies (Eqs. (23) and (25)) of the coupled model are consistent with the free frequencies of the decoupled models. The CW frequency of Eq. (23) is consistent with Eq. (81) of Coyette et al. (2016), provided that the effect of elastic deformations is neglected therein, whereas Eq. (25) is consistent with Eq. (3) of Baland et al. (2011), since $(C - A)/C \simeq (C - A)/A$. The agreement in free modes between the coupled and decoupled models is due to the fact that the spin axis essentially remains fixed both in space in the CW mode (no precession) and with respect to the pole axis of the BF in the QDFW mode (no polar motion), so that the free modes of the coupled models are essentially decoupled, as we will see below.

For a fast rotator not locked in a Cassini state (e.g., the Earth), the CW and QDFW frequencies cannot be derived from the governing Eqs. (15–18) and therefore are not given by Eqs. (23–24), in the first-order approximation (see Appendix 2 for more details). Since the mean motion n of the Earth is smaller than its mean rotation rate Ω_o, it is reasonable to fully neglect the external torque to obtain the homogeneous system of equations, whereas a part of the torque remains in the case of a synchronous satellite. For the Earth, with $A = B$ and $h_z(0) = 0$, $\sigma_{\text{CW}} = \Omega_o(C - A)/A$ and the CW is a purely prograde mode of $\mathbf{m}$ (see Fig. 1). The QDFW degenerates into a purely retrograde mode of $\mathbf{p}$, also called the Tilt-Over Mode (TOM), with $\sigma_{\text{QDFW}} \rightarrow \sigma_{\text{TOM}} = \Omega_o$ in the BF (diurnal) and $\sigma'_{\text{TOM}} = 0$ in the IF (infinite period). The TOM is in fact a mathematical degeneracy of the free precession mode of finite period (about 26,000 years for the Earth), characterized by σ'_{FP} as given in Eqs. (126) or (131), and which is obtained by taking into account the small but homogeneous part of the external torque.

2.3 Eigenmodes

The CW mode can be written either as an elliptical motion

$$p_x \simeq m_x = c_{\text{CW}} \cos(\sigma_{\text{CW}} t + \phi_{\text{CW}}), \tag{26}$$

$$p_y \simeq m_y = c_{\text{ell}} c_{\text{CW}} \sin(\sigma_{\text{CW}} t + \phi_{\text{CW}}), \tag{27}$$

or as a sum of prograde and circular retrograde motions at frequency σ_{CW}

$$p_x \simeq m_x = c_{\text{CW}} \left(\frac{1 + c_{\text{ell}}}{2} \cos(\sigma_{\text{CW}} t + \phi_{\text{CW}}) + \frac{1 - c_{\text{ell}}}{2} \cos(-\sigma_{\text{CW}} t - \phi_{\text{CW}}) \right), \tag{28}$$

$$p_y \simeq m_y = c_{\text{CW}} \left(\frac{1 + c_{\text{ell}}}{2} \sin(\sigma_{\text{CW}} t + \phi_{\text{CW}}) + \frac{1 - c_{\text{ell}}}{2} \sin(-\sigma_{\text{CW}} t - \phi_{\text{CW}}) \right). \tag{29}$$

The transformation between elliptic and circular formulation is a simple matter of trigonometric manipulations. The factor c_{ell} can be approximated as

$$c_{\text{ell}} \simeq \sqrt{\frac{4(C - A)n + h_z(0)}{(C - B)n + h_z(0)}} \neq 1, \tag{30}$$

and accounts for the ellipticity of the free trajectory's which is mainly due to the synchronous rotation (see the factor 4 in the numerator instead of 1 in the non-synchronous case), but also

to the difference between A and B. c_{CW} and ϕ_{CW} are arbitrary constants depending on the initial conditions. The CW mode corresponds to quasi-identical free motions in $\mathbf{m}$ and $\mathbf{p}$, since the spin axis remains essentially fixed with respect to inertial space in that mode. This can be verified with Euler's equation (14) which reduces to $p \simeq m$ for both the prograde and circular retrograde components since $\sigma_{CW}/n \ll 1$.

In the QDFW mode, the Laplace pole motion with respect to the BF is quasi-circular and retrograde and much larger than the free polar motion:

$$m_x \ll p_x \simeq c_{QDFW} \cos(-\sigma_{QDFW}t - \phi_{QDFW}), \tag{31}$$

$$m_y \ll p_y \simeq c_{QDFW} \sin(-\sigma_{QDFW}t - \phi_{QDFW}). \tag{32}$$

This mode therefore essentially represents the quasi-diurnal motion of the spin axis and BF axis with respect to the Laplace pole. c_{QDFW} and ϕ_{QDFW} are arbitrary constants depending on the initial conditions. The fact that $p \gg m \simeq 0$ can also be seen from Euler's equation (14) for $\sigma_{QDFW} \simeq -n$ for the retrograde motion. For the prograde motion, $\sigma_{QDFW} \simeq n$, and Euler's equation shows hat $m \simeq 2p \simeq 0$.

2.4 Forced solution

In this section, we describe the main characteristics of the numerical solution for the orientation of our Titan toy model, presented in Fig. 2. We also derive an approximate analytical solution for the orientation of a synchronous satellite, and compare it to the numerical solution (panels (a) and (b) of Fig. 3). The difference between the analytical coupled solution and the decoupled solutions of Coyette et al. (2016) and Baland et al. (2011) for the polar motion (m_x, m_y) and spin precession (s_x, s_y) is shown in panels (c) and (d) of Fig. 3, respectively.

2.4.1 Form of the solution

As the system composed of Eqs. (15–18) can be solved for each frequency of the forcing, we express the full solution for polar motion and Laplace pole motion in the BF as

$$\begin{pmatrix} m_x \\ m_y \\ p_x \\ p_y \end{pmatrix} = \begin{pmatrix} m_x \\ m_y \\ p_x \\ p_y \end{pmatrix}_{ext} + \begin{pmatrix} m_x \\ m_y \\ p_x \\ p_y \end{pmatrix}_{off} + \begin{pmatrix} m_x \\ m_y \\ p_x \\ p_y \end{pmatrix}_{atm}, \tag{33}$$

where the first, second, and third terms correspond to the part of the solution related to the external forcing by the parent planet, the constant terms, and the periodic terms of the atmospheric forcing, respectively.

In the Earth rotation community, the motion of the spin axis in space is usually seen as the motion with respect to a frame attached to the BF equator of a reference time (for instance, the J2000 epoch). It is represented in the form of nutations $\Delta\epsilon$ in orbital obliquity and $\Delta\psi$ in node longitude (e.g., Defraigne et al. 1995). The projection, in Cartesian coordinates, of the trajectory of the spin axis onto the J2000 equator, $(x, y) = (\sin\varepsilon_0\Delta\psi, \Delta\varepsilon)$ with ε_0 the initial obliquity, is a composition of prograde and retrograde circular motions. For each circular component, the nutations in obliquity and in longitude are therefore shifted by $\pi/2$ with respect to each other, and the amplitude of the nutation in longitude equals to that of the nutation in obliquity, normalized by the sinus of the initial obliquity. We adapt that kind of representation to the case of synchronous bodies in the Cassini state, considering the Laplace
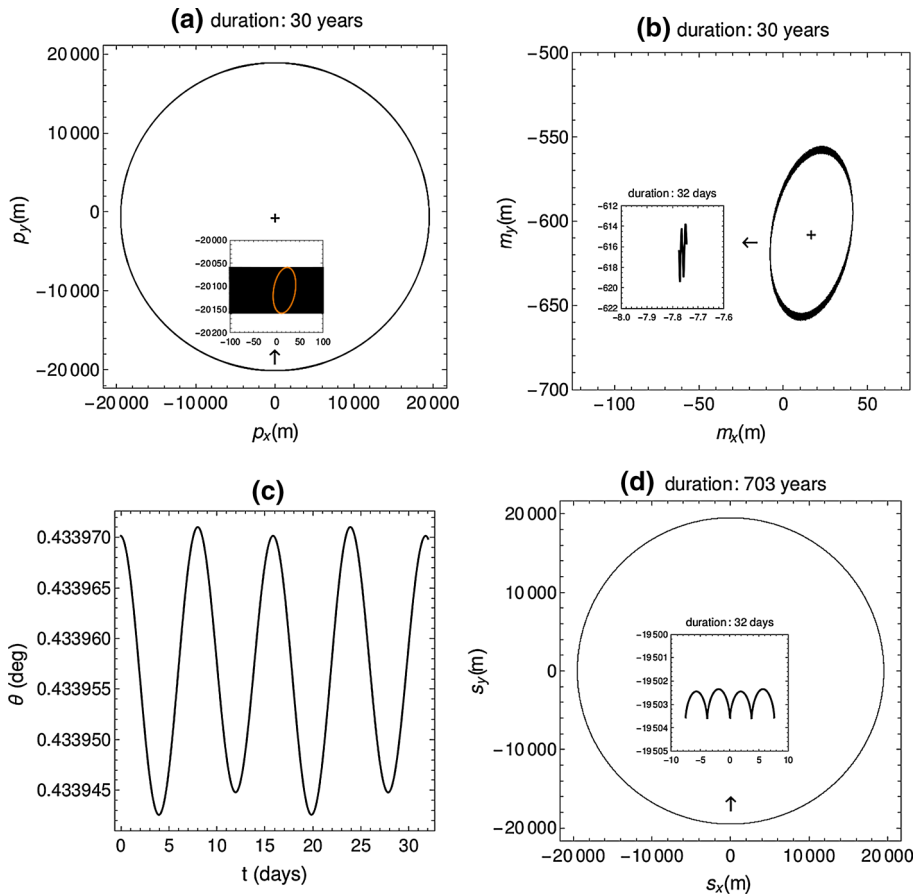
Fig. 2 Numerical solution for the Titan toy model. Panels **a** and **b** describe the evolution over 30 years of the equatorial components of the unit vector along the Laplace plane $\mathbf{p} = (p_x, p_y)$ and of the unit vector along the spin axis $\mathbf{m} = (m_x, m_y)$, as distances in meters at the surface of the satellite. The offset due to the constant terms of the atmospheric forcing is materialized by the cross markers. The evolution of $\mathbf{p}$ is quasi-circular, diurnal, and mainly governed by the external torque, whereas the evolution of $\mathbf{m}$ is elliptical, annual, and mainly governed by the atmospheric torque. The trajectory of $\mathbf{p}$ is covered about 700 times over 30 years, each circle being slightly shifted with respect to the previous one because of the annual atmospheric torque, explaining the thickness of the curve in panel (**a**). To highlight the annual Laplace pole motion, we zoom on one region, consider times equally spaced by a diurnal cycle, and join the corresponding points to draw an ellipse of quasi the same dimensions as the ellipse of the annual polar motion. The zoomed region in panel (**b**) highlights the quasi-diurnal external component of the solution for $\mathbf{m}$. Panel **c** displays the evolution over two diurnal cycles ($\simeq 32$ days) of the inertial obliquity θ, where one can easily see the semi-diurnal variations due to the external gravitational torque. The diurnal variations associated with the atmospheric torque are an order of magnitude smaller than the externally driven nutations. The trajectory of the unit vector along the spin axis projected onto the Laplace plane (s_x, s_y) is shown in panel (**d**) over the duration of the orbital precession (703 years) which drives the spin precession. The zoomed area displays the small semi-diurnal external and diurnal atmospheric nutations

plane as the reference plane. We consider the inertial obliquity θ, the angle between the rotation axis and the Laplace pole (see Fig. 10) which can be computed as $\theta \simeq |\mathbf{m} - \mathbf{p}|$. In the following, we show that

$$\theta \simeq \bar{\theta} + \Delta\theta_{\text{ext}} + \sum_{\varpi \neq 0} \Delta\theta_{\text{atm}}(\varpi), \tag{34}$$

where $\bar{\theta}$ is the mean inertial obliquity. The longitude of the ascending node of the rotation frame (see Fig. 10) can be written as:

$$\xi \simeq \Omega + \Delta\xi_{\text{ext}} + \sum_{\varpi \neq 0} \Delta\xi_{\text{atm}}(\varpi), \tag{35}$$

with Ω the longitude of the ascending node of the orbital plane. $\Delta\theta_{\text{ext/atm}}$ and $\Delta\xi_{\text{ext/atm}}$ are obliquity/longitude nutations due to the external gravitational torque or to the periodic atmospheric forcing. The equatorial components (s_x, s_y) of the unit vector along the spin axis expressed in the coordinates of the IF (see Eq. (102), Appendix 1) can be written, at first order in obliquity and longitude nutations, as

$$s_x \simeq \theta \sin\Omega + \bar{\theta}\,(\xi - \Omega)\cos\Omega, \tag{36}$$
$$s_y \simeq -\theta \cos\Omega + \bar{\theta}\,(\xi - \Omega)\sin\Omega. \tag{37}$$

The prograde and retrograde decomposition naturally also applies to (s_x, s_y), so that for each circular component, the amplitude of a given nutation in longitude is equal to that of the nutation in obliquity, normalized by the mean inertial obliquity.

2.4.2 Numerical results for the Titan toy model

The main feature is the quasi-circular retrograde Laplace pole motion (panel a in Fig. 2) with a radius of about 19.3 km measured at the surface of Titan, which is essentially driven by the external gravitational forcing by Saturn (see below). The polar motion (panel b) is elliptical, reaches a few tens of meters in amplitude, and is mainly induced by the annual atmospheric forcing. The centers of polar motion and of Laplace pole motion are offset (**polar offset** in the following) by a few hundred meters from zero because of the constant term of the atmospheric forcing.

Numerical results, for **m** and **p**, derived with the analytical solutions given below, are summarized in Table 3, in both elliptical and circular pro/retrograde forms. In the pro/retrograde form, the ratio of the externally driven **p** and **m** solutions ($w = \pm(n - \dot{\Omega}) \simeq \pm n$) are 2 and $\ll 1$, respectively, as must be according to Euler's kinematic Eq. (14). The ratio is $\simeq 1$ for the annual atmospheric solution, since $|w| = \varpi_{an} \ll n$, and exactly 1 for the constant atmospheric solution, since $w = 0$. This shows that the externally driven, essentially retrograde, Laplace pole motion has only a very small polar motion counter part, and that the atmospherically driven polar motion and Laplace pole motion are of the same order of magnitude (see Table 3).

The behavior of the spin axis as seen from the IF can be inferred from the circular pro/retrograde decomposition of the solutions for **m** and **p**. Each circular component of the solution expressed in the BF at a frequency w, and of amplitudes m and p, corresponds to a circular motion of the rotation axis with respect to the Laplace pole of frequency $w + n$ and of amplitude $|m - p|$ in the IF. The large retrograde and quasi-diurnal external Laplace pole motion in the BF corresponds to a large nutation in the IF at the orbital precession period, which is in fact the main precession of the spin axis, characterized by an inertial obliquity of 0.43° (see panels c and d in Fig. 2). The small prograde external solution in the BF corresponds to a small semi-diurnal nutation in the IF. The atmospheric solution at annual period corresponds to quasi-diurnal nutations in the IF, which have a very small amplitude. The polar offset has no influence on spin motion seen from space.

Table 3 Amplitudes and frequencies of the different parts of the solution of Eq. (33) for the Titan toy model of Table 1, in elliptical and pro/retrograde circular forms

Solution form			Ext.	Atm.	Atm.
Elliptical		Freq. BF	$n - \dot{\Omega}$	0	ϖ_{an}
		m_x	$\simeq 0$ m	16.7 m	-24.53 m
		m_y	2.4 m	-607.2 m	-49.52 m
		p_x	19.3 km	16.7 m	-24.46 m
		p_y	19.3 km	-607.2 m	-49.49 m
Circular	→ Prograde	Freq. BF	$n - \dot{\Omega}$	0	ϖ_{an}
		m_p	1.2 m	303.6 m	36.76 m
		p_p	0.6 m	303.6 m	36.71 m
		$|m_p/p_p|$	2	1	$\simeq 1$
		Freq. IF	$2n - \dot{\Omega}$	n	$n + \varpi_{an}$
		Amp. IF	0.6 m	0 m	0.05 m
	→ Retrograde	Freq. BF	$-n + \dot{\Omega}$	0	$-\varpi_{an}$
		m_r	-1.2 m	303.6 m	13.25 m
		p_r	-19.3 km	303.6 m	13.27 m
		$|m_r/p_r|$	$\ll 1$	1	$\simeq 1$
		Freq. IF	$\dot{\Omega}$	n	$n - \varpi_{an}$
		Amp. IF	19.3 km	0 m	0.02 m

The latter form verifies Euler kinematic Eq. (14) and allows to easily transform the solution to the IF, since the amplitude in the IF is the difference $|m - p|$ in amplitudes in the BF

2.4.3 Analytical solution related to the external forcing by the parent planet

The solution at the quasi-diurnal frequency $f = (n - \dot{\Omega})$ in the BF corresponding to the external torque can be written, with the numerator correct up to the first order in $(C - A)/B$ and in $\dot{\Omega}/n$, in elliptical form as

$$\begin{pmatrix} m_x \\ m_y \\ p_x \\ p_y \end{pmatrix}_{ext} \simeq -\frac{\theta_0}{n} \begin{pmatrix} 0 \\ 2\dot{\Omega}\cos(M + \omega) \\ (n - 2\dot{\Omega})\sin(M + \omega) \\ (n - \dot{\Omega})\cos(M + \omega) \end{pmatrix}, \tag{38}$$

$$\theta_0 = -\frac{3\frac{C-A}{B}in^4}{(f^2 - \sigma_{CW}^2)(f^2 - \sigma_{QDFW}^2)}, \tag{39}$$

with σ_{CW} and σ_{QDFW} given by Eqs. (23–24), and shows resonances with the CW and the QDFW. The solution is resonantly amplified by the QDFW, as can be seen by writing the resonance factor in θ_o as proportional to $1/(\dot{\Omega} + \sigma_{FP}')$, if the free precession period is close enough to the orbital precession period in space (e.g., for the toy model, it is amplified by 36%, compared to a case where $\dot{\Omega} \ll \sigma_{FP}'$). It cannot be amplified by a resonance with the CW mode, since the CW period is very long (> 100 years for the toy model) compared to the forcing period ($\simeq 16$ days).

By trigonometric manipulations, one can see that the amplitude of the prograde Laplace pole motion $p_p^{ext} = \theta_0\dot{\Omega}/2n$ is much smaller than the amplitude of the retrograde motion $p_r^{ext} = -\theta_0(2n - 3\dot{\Omega})/2n$ (see Table 3). The polar motion, essentially along the y-axis of
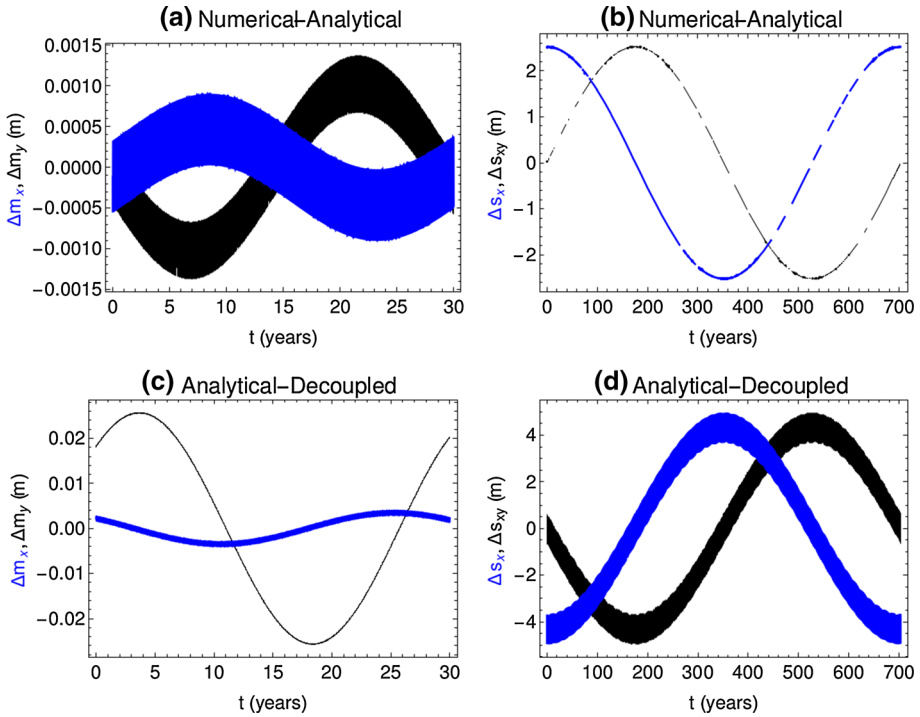
Fig. 3 Differences in meters at the surface between the numerical and analytical solutions of the coupled models (top panels) and between the analytical solution of the coupled models and the solution of the decoupled models (bottom panels) for a rigid solid Titan. Left panels: differences in polar motion. Right panels: differences in spin precession. The difference between the numerical and analytical annual coupled solutions for Titan's annual polar motion due to the atmospheric torque is < 0.002 m, see panel (**a**). The analytical solution for the annual polar motion of the coupled model is in good agreement (to 0.1%, see panel **c**) with the solution obtained from Eqs. (84–85) of Coyette et al. (2016). Due to the external gravitational torque only, the analytical coupled solution differs by 2.5 m in mean obliquity with respect to the numerical solution, see the large oscillations in panel (**b**). The difference between the mean inertial obliquity of the decoupled model of Baland et al. (2011) and the mean inertial obliquity of the analytical solution of the coupled model is 4.3 m and explains the amplitude of the large oscillations in panel (**d**). As the decoupled solution of Baland et al. (2011) neglects nutation induced by the coupling with the polar motion, semi-diurnal oscillations of 0.6 m amplitude, due to the external torque can also be seen in panel (**d**). Nutations related to the atmosphere are an order of magnitude smaller

the Body Frame, and of amplitude $-2\theta_0\dot{\Omega}/n$, corresponds to a combination of prograde and retrograde motions with amplitude $m_{p/r}^{\text{ext}} = \pm\theta_0\dot{\Omega}/n$. The difference between the numerical and analytical solutions for the diurnal polar motion can be seen as the diurnal oscillations in panel (a) of Fig. 3, and is four orders of magnitudes below the amplitude of the solution.

Injecting Eq. (38) in Eq. (101) for θ, and expanding the result up to the first order in $\dot{\Omega}/n$, the mean inertial obliquity is given by

$$\bar{\theta} = \theta_0\left(1 - \frac{5}{2}\frac{\dot{\Omega}}{n}\right) \tag{40}$$

and the semi-diurnal nutations in obliquity and longitude can be expressed as

$$\{\Delta\theta_{\text{ext}}, \bar{\theta}\Delta\xi_{\text{ext}}\} = -\frac{\theta_0}{2}\frac{\dot{\Omega}}{n}\{\cos 2(M+\omega), \sin 2(M+\omega)\}. \tag{41}$$

From Eqs. (40–41), we determine the motion of the spin axis in space related to the external gravitational torque by using Eqs. (36–37):

$$s_x^{\text{ext}} \simeq \bar{\theta} \sin \Omega - \frac{\theta_0}{2} \frac{\dot{\Omega}}{n} \sin(2(M + \omega) + \Omega) \tag{42}$$

$$s_y^{\text{ext}} \simeq -\bar{\theta} \cos \Omega + \frac{\theta_0}{2} \frac{\dot{\Omega}}{n} \cos(2(M + \omega) + \Omega). \tag{43}$$

The frequencies of the variations in $s_{x/y}^{\text{ext}}$ are $\dot{\Omega}$ and $(2n - \dot{\Omega})$, and their amplitudes correspond to the differences $(m_r - p_r)$ and $(m_p - p_p)$ of the retrograde and prograde amplitudes, respectively (see Table 3). The decomposition of $(s_x^{\text{ext}}, s_y^{\text{ext}})$ into a main precession and a secondary semi-diurnal nutation also appears in Eqs. (67–68) of Varadi et al. (2005).

Note that the inertial obliquity varies with time about a mean value $\bar{\theta} \neq \theta_0$. If we restrict the second factor in Eq. (38) to order zero in $\dot{\Omega}/n$, which amounts to neglecting the polar motion and nutations, we get $\bar{\theta} = \theta_o$. This corresponds to a constant over time obliquity $\eta_0 = (\theta_0 - i)$ (0.114° for the toy model) which, by neglecting σ_{CW} and $\dot{\Omega}$ with respect to n in Eq. (39) for θ_0, can be written as

$$\eta_0 \simeq \frac{-i\dot{\Omega}}{\dot{\Omega} + \sigma_{\text{FP}}'}. \tag{44}$$

This expression is identical to the solution of Baland et al. (2011) obtained in a decoupled model where the polar motion has been assumed to be zero. Like the nutations, the difference $(\bar{\theta} - \theta_0)$ in Eq. (40) is therefore the result of the coupling between the spin precession and the polar motion. For Titan, see Fig. 3, both $(\bar{\theta} - \theta_0)$ and the nutations are smaller than the actual measurement precision of about 1 km (Meriggiola et al. 2016). The decoupled solution of Baland et al. (2011) is therefore an excellent approximation.

Using Eq. (44), we now express the y-component of the polar motion as a function of η_o

$$m_y^{\text{ext}} \simeq \frac{3n^2(C - A)}{A(n^2 - \sigma_{\text{CW}}^2)} \eta_0 \cos(M + \omega). \tag{45}$$

This expression is similar to the solution of Coyette et al. (2016) for the diurnal polar motion forced by the parent planet.[3] The difference between our solution for m_y^{ext} of Eq. (38) and the one of Coyette et al. (2016) (or of Eq. 45) is so small that they cannot be distinguished in panel (c) of Fig. 3, due to the larger annual oscillations (see below). This good agreement is due to the fact that the obliquity η_0 is negligibly influenced by the polar motion itself.

2.4.4 Analytical solution related to the atmospheric forcing

The solution corresponding to the constant term of the atmospheric forcing (the polar offset) is given by

$$\begin{pmatrix} m_x \\ m_y \end{pmatrix}_{\text{off}} = \begin{pmatrix} p_x \\ p_y \end{pmatrix}_{\text{off}} \simeq \begin{pmatrix} \frac{h_x(0)}{4(C-A)n + h_z(0)} \\ \frac{h_y(0)}{(C-B)n + h_z(0)} \end{pmatrix}, \tag{46}$$

---

[3] See their Eqs. (85, 92–93) where ϖ must be replaced by $(n - \dot{\Omega})$. Note that a factor 3 is missing (typo) in the terms proportional to the obliquity η in their Eqs. (92–93). Numerical results presented therein are correct. Note also that Coyette et al. (2016) find a 6 m amplitude for the diurnal polar motion excited by the parent planet, whereas we obtain an amplitude of 2.4 m. This is because they use the measured obliquity (0.32°) and not the predicted solid obliquity (0.11°) as we implicitly do within the coupled model.

in total agreement with Eqs. (82–83) of Coyette et al. (2016). The solution for $\mathbf{m}_{\text{off}}$ reflects the balance reached by the spin axis between the orientation of the atmospheric angular momentum and the orientation of the axis of highest inertia along which the rotation would be stable if no torque was applied. The polar offset increases with decreasing flattenings, so that the spin axis tends to align with the atmospheric angular momentum axis in the limit case of a spherical body. As already anticipated in Sect. 2.4.2, both axes (rotation and Laplace) share the same offset, as follows from Euler's equation Eq. (14) for $w = 0$, and there is no effect in inertial obliquity θ computed from Eq. (101) and in spin motion seen from space. This is why there is no contribution of the polar offset in Eqs. (36–37). This can also be understood from the fact that, seen from the IF, the forcing is at short period (diurnal) compared to the FP (185 years), while seen from the BF, the forcing is at long period (infinite) compared to the CW (116 years). As a result, the spin axis is able to follow the forcing in the BF ($\mathbf{m}_{\text{off}} \neq 0$), but not in the IF where it stays fixed ($\mathbf{m}_{\text{off}} = \mathbf{p}_{\text{off}}$).

The solution corresponding to the periodic terms of the atmospheric forcing can be expressed as a sum of elliptical motion with amplitudes and phases given in Appendix 3 as functions of those of the atmospheric forcing of Eq. (8), or as a sum of prograde and retrograde circular motions

$$\begin{pmatrix} m_x \\ m_y \\ p_x \\ p_y \end{pmatrix}_{\text{atm}} \simeq \sum_{\varpi \neq 0} \begin{pmatrix} m_p(\varpi)\cos(\varpi t + \phi_p(\varpi)) + m_r(\varpi)\cos(-\varpi t - \phi_r(\varpi)) \\ m_p(\varpi)\sin(\varpi t + \phi_p(\varpi)) + m_r(\varpi)\sin(-\varpi t - \phi_r(\varpi)) \\ p_p(\varpi)\cos(\varpi t + \phi_p(\varpi)) + p_r(\varpi)\cos(-\varpi t - \phi_r(\varpi)) \\ p_p(\varpi)\sin(\varpi t + \phi_p(\varpi)) + p_r(\varpi)\sin(-\varpi t - \phi_r(\varpi)) \end{pmatrix}, \quad (47)$$

with amplitudes ($m_{p/r}(\varpi)$, $p_{p/r}(\varpi)$) and phases ($\phi_{p/r}(\varpi)$). For long forcing periods ($\varpi \ll n$), p_x^{atm} and p_y^{atm} tend to be close to m_x^{atm} and m_y^{atm}, respectively, as shown by Euler's Eq. (14), so that the atmosphere changes the orientation of the BF, but does not affect the orientation of the rotation axis in space. Table 3 gathers results for the Titan toy model. The difference between the numerical and analytical annual coupled solutions for atmospheric polar motion is very small (see panel (a) of Fig. 3), whereas the solution of Coyette et al. (2016) for the annual polar motion is a very good approximation (panel c).

The periodic atmospheric forcing causes small nutations of the spin axis in space. Injecting Eqs. (38) and (47) in Eq. (101) for θ, at first order in $\dot{\Omega}/n$, $m_{p/r}$ and $p_{p/r}$, we have

$$\Delta\theta_{\text{atm}}(\varpi) = (m_p(\varpi) - p_p(\varpi))\sin(M + \omega + \varpi t + \phi_p(\varpi))$$
$$+ (m_r(\varpi) - p_r(\varpi))\sin(M + \omega - \varpi t - \phi_r(\varpi)), \quad (48)$$
$$\bar{\theta}\Delta\xi_{\text{atm}}(\varpi) = (p_p(\varpi) - m_p(\varpi))\cos(M + \omega + \varpi t + \phi_p(\varpi))$$
$$+ (p_r(\varpi) - m_r(\varpi))\cos(M + \omega - \varpi t - \phi_r(\varpi)), \quad (49)$$

for the nutation related to the atmospheric torque at frequency ϖ. The motion of the spin axis in space due to the atmospheric forcing can be obtained from the nutations of Eqs. (48) and (49) by using Eqs. (36–37)

$$s_x \simeq \sum_{\varpi \neq 0} (p_p(\varpi) - m_p(\varpi))\cos(M + \omega + \Omega + \varpi t + \phi_p(\varpi)) \quad (50)$$

$$+ (p_r(\varpi) - m_r(\varpi))\cos(M + \omega + \Omega - \varpi t - \phi_r(\varpi)), \quad (51)$$

$$s_y \simeq \sum_{\varpi \neq 0} (p_p(\varpi) - m_p(\varpi))\sin(M + \omega + \Omega + \varpi t + \phi_p(\varpi)) \quad (52)$$

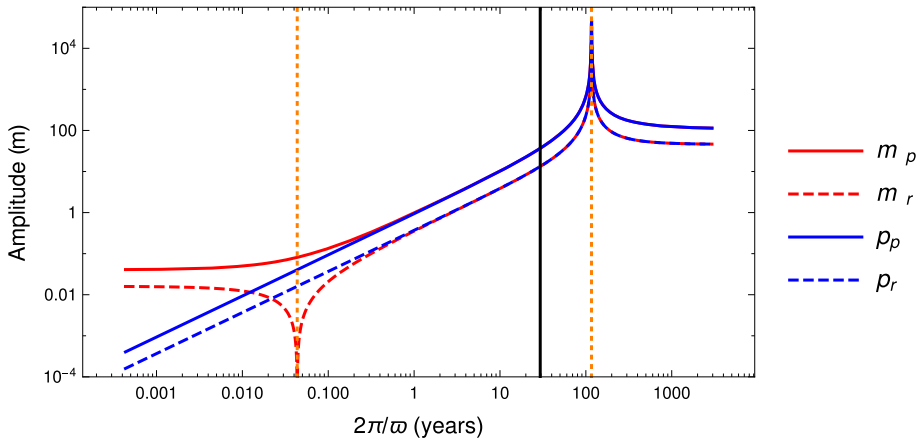$$+ (p_r(\varpi) - m_r(\varpi))\sin(M + \omega + \Omega - \varpi t - \phi_r(\varpi)). \quad (53)$$

Fig. 4 Amplitudes of the atmosphere contribution to the prograde and retrograde parts of the solution for the PM and Laplace pole motion, as a function of the forcing period, assuming that the forcing amplitudes at any period are those of the annual forcing. The vertical black line is the annual period of the atmospheric forcing. The dashed orange lines are the QDFW and CW periods

For the annual atmospheric forcing, the frequencies of the atmospheric variations in $s_{x/y}$ are $n \pm \varpi_{an}$, as was already anticipated in Table 3. Their amplitudes are negligible (one order of magnitude smaller than the already small external nutations), confirming that the polar motion and spin precession can be seen as effectively decoupled from each other, even when the atmospheric torque is considered.

One may wonder whether it is possible to amplify the atmospheric PM to the detection level thanks to a resonant amplification, and to enhance the small atmospheric contribution to the spin precession at the same time. In our toy model, we have only considered annual atmospheric forcing, but there is a multitude of other atmosphere and lake forcings at other frequencies. To illustrate the behavior of the solution with respect to the forcing period, we vary the forcing period between a hundredth of the diurnal period and 100 times the annual period, without varying the forcing amplitudes and phases which are taken as those of the annual forcing. For periods larger than about 1 year, the spin and Laplace motion have similar amplitudes, as found above for the annual period (see Fig. 4). Forcings with period of about 100 years (or 3.5 Saturn revolution periods) are close enough to the CW period to produce a response with a significant amplification of both motions above the kilometer level. However, such periodic forcings are not likely to exist, as the atmosphere dynamics is governed by the revolution of Saturn around the Sun. For decreasing periods, the response tends to decrease and the difference between m_p and p_p and between m_r and p_r increases. For quasi-diurnal periods, $m_r \simeq 0$ (circular prograde polar motion). In principle, a resonance is possible if the forcing period is close enough to the QDFW period. However, an amplification of at least 4 (5) orders of magnitude is needed to reach the km level in PM (Laplace pole motion) and requires a very good match between frequencies, which is not so likely and depends on the atmospheric model chosen. Besides, in real conditions, such strong resonant amplifications would be counteracted by dissipative processes. We conclude that it is not possible to reach the detection limit in PM with a solid rigid model for Titan, in agreement with similar findings by Coyette et al. (2016) who consider a more realistic atmosphere dynamics. Similarly, the spin precession is very unlikely to be enhanced by an amplification of any atmospheric contribution.

3 Satellite with a subsurface ocean

3.1 A new set of variables

In studies of rotation of the Earth, it is customary to write one angular momentum equation for the whole body, one for the fluid outer core (FOC, subscript f), and one for the solid inner core (SIC, subscript s), all expressed in the BF of the mantle [see for instance the coupled system of equations (15a–15c) of Mathews et al. (1991)]. The variables to be solved for are all expressed in the coordinates of the mantle Body Frame (see Fig. 5), and are $\mathbf{m}$, the variations in rotation of the mantle with respect to the uniform rotation along the z-axis, normalized by the mean rotation rate, and $\mathbf{m}_f$ and $\mathbf{m}_s$, the normalized variations in rotation of the FOC and SIC, respectively, with respect to the mantle's rotation. Because the torque on the SIC depends on the tilt $\mathbf{n}_s$ between the z-axis of the mantle BF and the z-axis of the SIC BF, an additional kinematic equation governing this tilt is required to close the system (see Eq. (19) of Mathews et al. (1991)). Besides the two free modes related to variations in rotation rate, the system is characterized by four modes which are (1) the Chandler Wobble (CW), corresponding to a motion of the mantle rotation axis with respect to the mantle BF, and mainly associated with the variable $\mathbf{m}$, (2) the Free Core Nutation (FCN), corresponding to the motion of the fluid core rotation axis with respect to the mantle rotation axis, and mainly
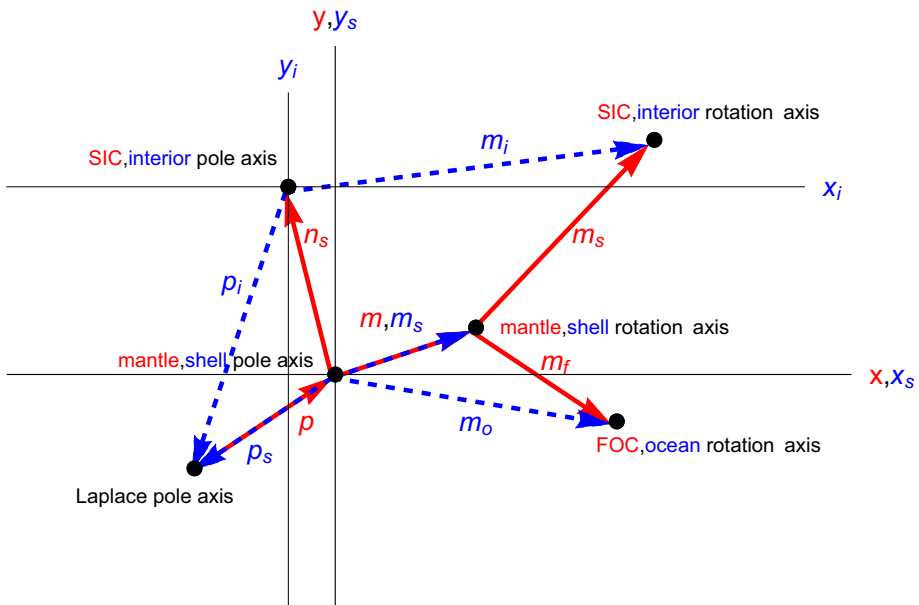

Fig. 5 Red: Rotation variables $\mathbf{m}$, $\mathbf{m}_f$, $\mathbf{m}_s$ and $\mathbf{n}_s$ projected onto the equator of the mantle BF (x, y), as defined by Mathews et al. (1991) to study Earth's rotation. The subscripts f and s stand for the fluid outer core and the solid inner core, respectively. The fifth variable $\mathbf{p}$ is introduced by Dumberry and Wieczorek (2016) to account for the effect of the precession of the Moon's mantle in space. Note that Dumberry and Wieczorek (2016) do not follow the convention sign of Eckhardt (1981) for $\mathbf{p}$. Blue: New set of rotation variables $\mathbf{m}_s$, $\mathbf{m}_o$, $\mathbf{m}_i$, $\mathbf{p}_s$ and $\mathbf{p}_i$ projected onto the equator of shell (x_s, y_s) or interior (x_i, y_i) BF. The subscripts s, o, and i stand for the shell, the ocean, and the interior, respectively. We here follow the convention sign of Eckhardt (1981) for the definition of $\mathbf{p}_s$ and $\mathbf{p}_i$

associated with the variable $\mathbf{m}_f$, (3) the Free Inner Core Nutation (FICN), corresponding to a motion of the inner core rotation axis with respect to the mantle rotation axis, and mainly associated with the variable $\mathbf{m}_s$, (4) the Inner Core Chandler Wobble (ICW), corresponding to a motion of the inner core rotation axis with respect to the inner core BF, associated with the combination of variables $\mathbf{m} + \mathbf{m}_s - \mathbf{n}_s$. The FCN and FICN both correspond to quasi-diurnal free wobbles in the BF. The FCN is also referred to as the NDFW (nearly diurnal free wobble) in the literature, even though they belong to different reference frames. The FICN is sometimes named PFCN (Prograde Free Core Nutation), as opposed to the FCN which is retrograde.

The precession of the Earth's mantle rotation axis with respect to the ecliptic plane, which is a good approximation of an inertial plane, is not included in the formalism of Mathews et al. (1991). As a result, the mantle rotation axis can be seen as fixed with respect to inertial space, so that the FCN and FICN can also be seen as motion of the FOC and SIC rotation axes with respect to inertial space. To properly study the coupling between spin motion axis in space and spin motion axis in the BF for synchronous satellites in the Cassini state, it is, however, necessary to account for the motion of the mantle rotation axis in space. The evolution of the tilt of the z-axis of the mantle with respect to the inertial space, denoted $\mathbf{p}$ (see Eq. 6), was introduced for the Moon by Eckhardt (1981) and was also used in Sect. 2 for an entirely solid satellite. It was also added as a fifth equation to the classical system for the Earth by Dumberry and Wieczorek (2016). With that additional equation comes a fifth free mode which is the Free Precession (FP) of the mantle spin axis in space, associated with the variable combination ($\mathbf{p} + \mathbf{m}$). The FCN and FICN are then associated with $\mathbf{p} + \mathbf{m} + \mathbf{m}_f$ and $\mathbf{p} + \mathbf{m} + \mathbf{m}_s$, respectively.

Instead of using the four variables classically used for the Earth extended with the variable $\mathbf{p}$, we choose to select five rotation variables showing more symmetry between the two solid layers and better suited to compare with previously developed more restricted models. We for example prefer not to use the tilt $\mathbf{n}_s$ but to use an equivalent variable as $\mathbf{p}$ for the solid interior, which is the combination $\mathbf{p} + \mathbf{n}_s$ (see Fig. 5). As the model in intended for icy satellites, we change the name of the layers and the associated subscripts. The mantle becomes the ice shell ($m \rightarrow s$), the FOC becomes the ocean ($f \rightarrow o$), and the SIC becomes the solid interior ($s \rightarrow i$). By analogy with Eckhardt's formalism for the solid case, we define a variable for the orientation of the Laplace pole in the BF of both the shell ($\mathbf{p}_s$) and of the interior ($\mathbf{p}_i$). We also define in a more symmetrical way variations of rotation for the shell ($\mathbf{m}_s$) and the interior ($\mathbf{m}_i$) with respect to their uniform rotation along the z-axis of their respective BF. As the ocean has no practically defined BF, we express the ocean rotation variations $\mathbf{m}_o$ in the coordinates of the shell BF. With our new set of variables, the system will be characterized by five free modes for the orientation of the rotation axes (see Table 4): the Chandler Wobble and the Interior Chandler Wobble which are defined by analogy with Earth's studies, the Free Precession (or QDFWs, the quasi-diurnal free wobble of the shell in the shell BF), the Free Ocean Nutation (or QDFWo in the shell BF) which replaces the FCN/NDFW of the Earth, and the Free Interior Nutation (or QDFWi in the interior BF) which replaces the FICN/PFCN of the Earth. In addition, there are two rotation rate free modes (the shell and interior free libration).

3.2 Angular momentum equations

The rotation of a synchronously rotating icy satellite with a global subsurface ocean is governed by the following five equations

Table 4 Free modes for a synchronous satellite with an internal global ocean, associated with our new set of rotation variables

Mode	Corresponding motion	Associated variables
CW	Shell rotation axis w.r.t shell BF	$\mathbf{m}_s$
ICW	Interior rotation axis w.r.t interior BF	$\mathbf{m}_i$
FP	Shell rotation axis w.r.t IF	
↪ QDFWs	Shell rotation axis w.r.t Laplace pole in shell BF	$\mathbf{m}_s - \mathbf{p}_s$
FON	Ocean rotation axis w.r.t IF	
↪ QDFWo	Ocean rotation axis w.r.t Laplace pole in shell BF	$\mathbf{m}_o - \mathbf{p}_s$
FIN	Interior rotation axis w.r.t IF	
↪ QDFWi	Interior rotation axis w.r.t Laplace pole in interior BF	$\mathbf{m}_i - \mathbf{p}_i$

$$\frac{\mathrm{d}\mathbf{H}_s}{\mathrm{d}t} + \mathbf{\Omega}_s \wedge \mathbf{H}_s = \mathbf{\Gamma}_s, \tag{54}$$

$$\frac{\mathrm{d}\mathbf{H}_{o(s)}}{\mathrm{d}t} + \mathbf{\Omega}_s \wedge \mathbf{H}_{o(s)} = \mathbf{\Gamma}_{o(s)}, \tag{55}$$

$$\frac{\mathrm{d}\mathbf{H}_i}{\mathrm{d}t} + \mathbf{\Omega}_i \wedge \mathbf{H}_i = \mathbf{\Gamma}_i, \tag{56}$$

$$\frac{\mathrm{d}\hat{p}_s}{\mathrm{d}t} + \mathbf{\Omega}_s \wedge \hat{p}_s = 0, \tag{57}$$

$$\frac{\mathrm{d}\hat{p}_i}{\mathrm{d}t} + \mathbf{\Omega}_i \wedge \hat{p}_i = 0. \tag{58}$$

Here, $\mathbf{H}_s$, $\mathbf{H}_{o(s)}$, and $\mathbf{H}_i$ are the angular momentum of the shell, ocean, and interior, $\mathbf{\Omega}_s$ and $\mathbf{\Omega}_i$ are the rotation vectors of the shell and of the interior. $\mathbf{\Gamma}_s$, $\mathbf{\Gamma}_{o(s)}$, and $\mathbf{\Gamma}_i$ are the torques exerted on the different layers. $\hat{p}_s$ and $\hat{p}_i$ are defined by analogy with the solid case (see Eq. 6):

$$\hat{p}_s = \begin{pmatrix} 0 \\ 0 \\ 1 \end{pmatrix} + \mathbf{p}_s = \begin{pmatrix} p_x^s \\ p_y^s \\ 1 \end{pmatrix} \quad \text{and} \quad \hat{p}_i = \begin{pmatrix} 0 \\ 0 \\ 1 \end{pmatrix} + \mathbf{p}_i = \begin{pmatrix} p_x^i \\ p_y^i \\ 1 \end{pmatrix}. \tag{59}$$

Vectors related to the shell or to the interior are expressed in the coordinates of their respective BF. The coordinate system (shell or interior BF) chosen to express vectors related to the ocean is indicated in parentheses in the subscripts. Here, the ocean's equation Eq. (55) is expressed in the coordinates of the shell BF.

In the next subsections, we determine expressions for the rotation, angular momentum and torque vectors. As the tidal deformations largely complexify the governing equations, we consider the solid layers to be rigid, as in Sect. 2. The main goal of this paper is to evaluate the effect of coupling between the different rotation quantities and to compare our results with those of studies in which the different rotation variables are studied independently of the other. Those decoupled studies have shown that the tidal effect is large for large icy satellites as Titan, but we do not expect that the inclusion of tides will change the conclusions of our comparisons. Inclusion of tides is foreseen in a follow-up paper.

3.3 Rotation vectors and angular momentum

The angular momentum of the solid layers (k stands here for s or i), in their respective BF, can be expressed similarly as Eq. (3) for the angular momentum of the solid satellite :

$$\mathbf{H}_k = \overline{\overline{I}}_k \mathbf{\Omega}_k, \tag{60}$$

with the inertia tensors and rotation vectors defined as Eq. (4) and Eq. (1), respectively:

$$\overline{\overline{I}}_k = \begin{pmatrix} A_k & 0 & 0 \\ 0 & B_k & 0 \\ 0 & 0 & C_k \end{pmatrix} \quad \text{and} \quad \mathbf{\Omega}_k = n \begin{pmatrix} 0 \\ 0 \\ 1 \end{pmatrix} + n\,\mathbf{m}_k = n \begin{pmatrix} m_x^k \\ m_y^k \\ 1 + m_z^k \end{pmatrix}, \tag{61}$$

with $m_z^k = \dot{\gamma}_k/n$. γ_k is the libration angle of layer k.

The development of the angular momentum of the ocean requires more care. As it is not practical to define a Body Frame for the ocean, whose mass distribution and orientation depends on the orientations of both the shell and interior, we choose to write the ocean angular momentum in the BF of an adjacent solid layer, in this case the shell BF. We model the relative velocity in the ocean as

$$\mathbf{v}_{o(s)} = (\mathbf{\Omega}_{o(s)} - \mathbf{\Omega}_s) \wedge \mathbf{r} + \mathbf{v}, \tag{62}$$

with $\mathbf{\Omega}_{o(s)}$ the rotation vector of the ocean, seen as a solid body rotation, and $\mathbf{r}$ the position vector. The additional velocity field $\mathbf{v}$ is a small field defined so that the total flow satisfies the boundary conditions at the non-spherical interfaces and so that $\mathbf{v}$ does not contribute to the ocean angular momentum. Such a simple flow is known as a Poincaré flow (e.g., Mathews et al. 1991, Eq. (6), where we have replaced $\mathbf{m}_f$ by $(\mathbf{\Omega}_{o(s)} - \mathbf{\Omega}_s)$, according to our choice of variables to solve for). Determining the exact expression for $\mathbf{v}$ in a three layer case would not be an easy task (in the biaxial case with no SIC, it is given after Eq. (B23) of Mathews et al. (1991); for a triaxial core-mantle boundary, see, e.g., Eq. (50) of Van Hoolst and Dehant (2002)), and is not necessary for computing the torque on the fluid layer, as we will see below. It is only needed to know that the components of $\mathbf{v}$ are proportional to the flattenings of the core-mantle and inner core boundaries, as noted by Mathews et al. (1991) in their Eq. (7).

We write the ocean rotation vector as

$$\mathbf{\Omega}_{o(s)} = n \begin{pmatrix} 0 \\ 0 \\ 1 \end{pmatrix} + n\,\mathbf{m}_o = n \begin{pmatrix} m_x^o \\ m_y^o \\ 1 + m_z^o \end{pmatrix}, \tag{63}$$

with $m_z^o = \dot{\gamma}_o/n$. Since the orientations of the two solid layers, and therefore also of the two interfaces of the ocean are different, we divide the ocean into a top (subscript ot) and a bottom (ob) part aligned with the shell and the interior, respectively. The boundary between the two parts is a sphere, which is therefore not affected by the orientation of the solid layers. As a result, the ocean angular momentum $\mathbf{H}_o$ can be written as the sum of the angular momentum of the top and bottom oceans. We express it here with respect to the reference frame attached to the shell:

$$\mathbf{H}_{o(s)} = \left(\overline{\overline{I}}_{ot(s)} + R_{(i \to s)} \overline{\overline{I}}_{ob(i)} R_{(i \to s)}^{-1} \right) \mathbf{\Omega}_{o(s)} \tag{64}$$

$$= n \begin{pmatrix} (A_{ot} + A_{ob})m_x^o + (C_{ob} - A_{ob})(p_x^s - p_x^i) \\ (B_{ot} + B_{ob})m_y^o + (C_{ob} - B_{ob})(p_y^s - p_y^i) \\ (C_{ot} + C_{ob})(1 + m_z^o) \end{pmatrix}. \tag{65}$$

Here $R_{(i \to s)}$ is the transformation matrix from the interior BF to the shell BF (see Eq. 108) and $\overline{\overline{I}}_{ot(s)}$ and $\overline{\overline{I}}_{ob(i)}$, the inertia tensor of the top and bottom oceans, are defined as in Eq. (61). The effect of the misalignment of the bottom ocean with respect to the shell and the top ocean is manifested by the presence of terms proportional to the components of the difference between $\mathbf{p}_s$ and $\mathbf{p}_i$. Similarly, the effect of the misalignment of the inner core of the Earth with respect to the mantle is present in the FOC angular momentum through the components of $\mathbf{n}_s$ (see Eq. (22a) of Mathews et al. (1991)), which would be the combination of $\mathbf{p}_s - \mathbf{p}_i$ if we were to define such a vector between the z-axes of the solid layers' BFs in the ocean case (see Fig. 5). Note that $(C_{ob} - A/B_{ob})$ and $(A/B/C_{ot} + A/B/C_{ob})$, and so $\mathbf{H}_{o(s)}$, do not depend on the radius of the sphere separating the top and bottom oceans, which can therefore be chosen arbitrarily between the largest radius of the triaxial solid interior and the smallest radius of the triaxial ocean–shell interface. This makes the decomposition of the ocean into a top and bottom fluid layer efficient and also intuitive.

3.4 Total torque on the ocean

The torque on the fluid layer includes the external gravitational torque (ext) by the parent planet, the internal torque (int) by the solid layers, and the hydrostatic (phs) and hydrodynamic (phd) pressure torques exerted at the ocean boundaries:

$$\mathbf{\Gamma}_{o(s)} = \mathbf{\Gamma}_{o,\text{ext}} + \mathbf{\Gamma}_{o,\text{int}} + \mathbf{\Gamma}_{o,\text{phs}} + \mathbf{\Gamma}_{o,\text{phd}}. \tag{66}$$

The different torques are formally defined as

$$\mathbf{\Gamma}_{o,\text{ext/int}} = -\int_{V_o} \mathbf{r} \wedge \rho_o \mathbf{\nabla} \Phi_{\text{ext/int}} \, dV, \tag{67}$$

$$\mathbf{\Gamma}_{o,\text{phs/phd}} = -\int_{S_o} (\mathbf{r}_o \wedge \hat{n}_o) P_{\text{hs/hd}}(\mathbf{r}_o) dS + \int_{S_i} (\mathbf{r}_i \wedge \hat{n}_i) P_{\text{hs/hd}}(\mathbf{r}_i) \, dS, \tag{68}$$

with Φ_{ext} the external gravitational potential of the parent planet and Φ_{int} the internal gravitational potential due to the shell and interior masses. The quantities $\mathbf{r}$, ρ_o, and V_o are the position vector, the density and the volume of the ocean; $\mathbf{r}_o$ and $\mathbf{r}_i$ are the position vectors of the points located on S_o and S_i, the ocean and interior surfaces; $\hat{n}_o$ and $\hat{n}_i$ are the outward unit normal on these surfaces.

We have divided the pressure P inside the ocean into a part P_{hs} corresponding to an ocean at rest (hydrostatic pressure), and a part P_{hd} which depends on the fluid motion (hydrodynamic pressure). The pressure gradient inside the ocean, which we assume to be inviscid, is given by the Navier–Stokes equation. In the coordinates of the shell BF, we have

$$\mathbf{\nabla} P = \mathbf{\nabla} P_{\text{hs}} + \mathbf{\nabla} P_{\text{hd}}, \tag{69}$$

with

$$\mathbf{\nabla} P_{\text{hs}} = -\rho_o \left(\mathbf{\nabla} \Phi_{\text{ext}} + \mathbf{\nabla} \Phi_{\text{int}} \right), \tag{70}$$

$$\mathbf{\nabla} P_{\text{hd}} = -\rho_o \left({}_s \wedge ({}_s \wedge \mathbf{r}) + \dot{}_s \wedge \mathbf{r} + 2{}_s \wedge \mathbf{v}_{o(s)} + \frac{d\mathbf{v}_{o(s)}}{dt} \right), \tag{71}$$

with $\frac{d\mathbf{v}_{o(s)}}{dt} = \frac{\partial \mathbf{v}_{o(s)}}{\partial t} + (\mathbf{v}_{o(s)}.\mathbf{\nabla})\mathbf{v}_{o(s)}$, the total derivative of the fluid velocity.

Applying Gauss theorem, the pressure torques can be alternatively written as

$$\mathbf{\Gamma}_{o,\text{phs/hd}} = -\int_{V_o} \mathbf{r} \wedge \mathbf{\nabla} P_{\text{hs/hd}} \, dV. \tag{72}$$

From Eqs. (67–72), it is straightforward to see that hydrostatic equilibrium implies

$$\boldsymbol{\Gamma}_{o,\text{ext}} + \boldsymbol{\Gamma}_{o,\text{int}} + \boldsymbol{\Gamma}_{o,\text{phs}} = 0 \tag{73}$$

and that the torque on the ocean, now written

$$\boldsymbol{\Gamma}_{o(s)} = \boldsymbol{\Gamma}_{o,\text{phd}}, \tag{74}$$

is only due to the hydrodynamic part of the pressure. This is not the case for the solid layers, as we will see below.

In the Earth rotation community, it is not customary to use the formal definition (Eq. 68) of $\boldsymbol{\Gamma}_{o,\text{phd}}$. As shown by Mathews et al. (1991) (see also Sasao et al. 1980), an alternative form for the angular momentum equation of the fluid layer can be obtained starting from the Navier–Stokes equation and involving the fact that $\mathbf{v}$ does not contribute to the angular momentum. They find that, in our notations:

$$\frac{d\mathbf{H}_{o(s)}}{dt} - n(\mathbf{m}_o - \mathbf{m}_s) \wedge \mathbf{H}_{o(s)} = 0. \tag{75}$$

This derivation is based on the knowledge that $\mathbf{v}$ is a quantity of first order in the flattenings of the fluid layer boundaries, but does not require to know the exact expression of $\mathbf{v}$. Therefore, comparing Eq. (55) with Eq. (75), the total torque on the ocean is given by

$$\boldsymbol{\Gamma}_{o(s)} = \boldsymbol{\Omega}_{o(s)} \wedge \mathbf{H}_{o(s)} \tag{76}$$

$$= n^2 \begin{pmatrix} (C_{ot} - B_{ot})m_y^o + (C_{ob} - B_{ob})(m_y^o + p_y^i - p_y^s) \\ -(C_{ot} - A_{ot})m_x^o - (C_{ob} - A_{ob})(m_x^o + p_x^i - p_x^s) \\ 0 \end{pmatrix}. \tag{77}$$

3.5 Total torque on the solid layers

The torques on the shell and on the solid interior can be written as

$$\boldsymbol{\Gamma}_s = \boldsymbol{\Gamma}_{s,\text{ext}} + \boldsymbol{\Gamma}_{s,\text{int}} + \boldsymbol{\Gamma}_{s,phs} + \boldsymbol{\Gamma}_{s,phd} + \boldsymbol{\Gamma}_{\text{atm}}, \tag{78}$$

$$\boldsymbol{\Gamma}_i = \boldsymbol{\Gamma}_{i,\text{ext}} + \boldsymbol{\Gamma}_{i,\text{int}} + \boldsymbol{\Gamma}_{i,phs} + \boldsymbol{\Gamma}_{i,phd}, \tag{79}$$

with $\boldsymbol{\Gamma}_{k,\text{ext}}$ the external gravitational torque by the parent planet on layer k, $\boldsymbol{\Gamma}_{k,\text{int}}$ the internal gravitational torque by the other layers and $\boldsymbol{\Gamma}_{k,\text{phs/phd}}$ the hydrostatic/hydrodynamic pressure torques exerted at the ocean boundary with layer k. The atmospheric torque on the shell $\boldsymbol{\Gamma}_{\text{atm}}$ is the same as in the solid case (see Eq. 8). The gravitational and pressure torques on solid layer k are formally defined as

$$\boldsymbol{\Gamma}_{k,\text{ext/int}} = -\int_{V_k} \mathbf{r} \wedge \rho_k \boldsymbol{\nabla} \Phi_{\text{ext/int}} \, dV, \tag{80}$$

$$\boldsymbol{\Gamma}_{s,\text{phs/phd}} = \int_{S_o} (\mathbf{r}_o \wedge \hat{n}_o) P_{\text{hs/hd}}(\mathbf{r}_o) dS = \int_{V_{ot}} \mathbf{r} \wedge \boldsymbol{\nabla} P_{\text{hs/hd}} \, dV, \tag{81}$$

$$\boldsymbol{\Gamma}_{i,\text{phs/phd}} = -\int_{S_i} (\mathbf{r}_i \wedge \hat{n}_i) P_{\text{hs/hd}}(\mathbf{r}_i) \, dS = \int_{V_{ob}} \mathbf{r} \wedge \boldsymbol{\nabla} P_{\text{hs/hd}} \, dV. \tag{82}$$

Because the hydrostatic pressure is directly related to the external and internal gravitational potential (Eq. 70), it is more convenient to write, for each solid layer, the sum of the gravitational torque and of the hydrostatic pressure torque as a gravitational torque corrected

for the effect of hydrostatic pressure, which acts as a transfer of the gravitational torques on the top and bottom ocean to the adjacent solid layers. Eqs. (78–79) are now written as

$$\mathbf{\Gamma}_s = \mathbf{\Gamma}_{s,\tilde{\text{ext}}} + \mathbf{\Gamma}_{s,\tilde{\text{int}}} + \mathbf{\Gamma}_{s,\text{phd}} + \mathbf{\Gamma}_{\text{atm}}, \tag{83}$$

$$\mathbf{\Gamma}_i = \mathbf{\Gamma}_{i,\tilde{\text{ext}}} + \mathbf{\Gamma}_{i,\tilde{\text{int}}} + \mathbf{\Gamma}_{i,\text{phd}}, \tag{84}$$

with

$$\mathbf{\Gamma}_{s,\tilde{\text{ext}}/\tilde{\text{int}}} = -\int_{V_{s+ot}} \mathbf{r} \wedge \rho(\mathbf{r}) \nabla \Phi_{\text{ext/int}} \, dV, \tag{85}$$

$$\mathbf{\Gamma}_{i,\tilde{\text{ext}}/\tilde{\text{int}}} = -\int_{V_{i+ob}} \mathbf{r} \wedge \rho(\mathbf{r}) \nabla \Phi_{\text{ext/int}} \, dV. \tag{86}$$

By analogy with the solid case (see Eq. 5), the external gravitational torques, including the effect of hydrostatic pressure, are written as in Eqs. (109–110). The expressions for the internal torques, including the effect of the hydrostatic pressure, are given by Eq. (111), see Appendix 1.

From a comparison of Eq. (72) for the formal expression of the hydrodynamic pressure torque on the ocean and Eqs. (81–82) for the formal expressions of the hydrodynamic pressure torques on the shell and on the solid interior, it follows that

$$\mathbf{\Gamma}_{s,\text{phd}} + \mathbf{\Gamma}_{i,\text{phd}} + \mathbf{\Gamma}_{o,\text{phd}} = 0. \tag{87}$$

Making use of the final expression for the hydrodynamic pressure torque on the ocean of Eq. (76), we obtain

$$\mathbf{\Gamma}_{s,\text{phd}} = -\mathbf{\Omega}_{o(s)} \wedge \mathbf{H}_{ot(s)} = -n^2 \begin{pmatrix} (C_{ot} - B_{ot})m_y^o \\ -(C_{ot} - A_{ot})m_x^o \\ 0 \end{pmatrix}, \tag{88}$$

$$\mathbf{\Gamma}_{i,\text{phd}} = -\mathbf{\Omega}_{o(s)} \wedge \mathbf{H}_{ob(s)} = -n^2 \begin{pmatrix} +(C_{ob} - B_{ob})(m_y^o + p_y^i - p_y^s) \\ -(C_{ob} - A_{ob})(m_x^o + p_x^i - p_x^s) \\ 0 \end{pmatrix}. \tag{89}$$

At first order in small quantities, $\mathbf{\Gamma}_{i,\text{phd}}$ has the same expression in the interior BF as in the shell BF, so that Eq. (89) which is written in the shell BF can be injected in Eq. (56) which is written in the interior BF.

3.6 Final system

Making use of Eqs. (76,83,84) for the torques on the different layers, the system of vector Eqs.(54–58) is expanded into 13 scalar equations subdivided into two independent sets.

A first set of three equations governs librations and LOD variations

$$C_s n \ddot{\gamma}_s - 3n^2[(B_s - A_s) + (B_{ot} - A_{ot})](s - \gamma_s) - n\kappa_{\text{int}}^z(\gamma_s - \gamma_i) = \tilde{\Gamma}_z, \tag{90}$$

$$C_o n \ddot{\gamma}_o = 0, \tag{91}$$

$$C_i n \ddot{\gamma}_i - 3n^2[(B_i - A_i) + (B_{ob} - A_{ob})](s - \gamma_i) + n\kappa_{\text{int}}^z(\gamma_s - \gamma_i) = 0. \tag{92}$$

We refer the reader to Van Hoolst et al. (2013) and Coyette et al. (2018) for a presentation of the solution of these equations.

The equations governing polar motion and precession form a system of ten equations that can be written as

$$\dot{\mathbf{u}} + \mathbf{K}\mathbf{u} = \mathbf{T}, \tag{93}$$

with

$$
\mathbf{u} = \begin{pmatrix} m_x^s \\ m_y^s \\ m_x^o \\ m_y^o \\ m_x^i \\ m_y^i \\ p_x^s \\ p_y^s \\ p_x^i \\ p_y^i \end{pmatrix}, \quad \mathbf{T} = \begin{pmatrix} \frac{h_y(0)}{A_s} + \frac{\tilde{\Gamma}_x}{n A_s} \\ -\frac{h_x(0)}{B_s} + \frac{\tilde{\Gamma}_y}{n B_s} + 3n \frac{(A_{s+ot} - C_{s+ot})}{B_s} i \sin(\omega + M - \pi) \\ 0 \\ 0 \\ 0 \\ 3n \frac{(A_{i+ob} - C_{i+ob})}{B_i} i \sin(\omega + M - \pi) \\ 0 \\ 0 \\ 0 \\ 0 \end{pmatrix}, \quad (94)
$$

and the components of the matrix **K** are given in Appendix 4. **u** is the vector of the 10 unknowns: the equatorial components of the variations in rotation of the shell, ocean, and interior with respect to the uniform rotation along the z-axis of the shell or interior BF and of the unit vector along the Laplace pole expressed with respect to the shell and interior BFs. The vector **T** contains the parts of the torques which do not depend on the variables to be solved for. The remaining parts of the torque are included in the product (**Ku**), along with the cross product terms of the governing equations.

We aim to compare the solution of this coupled model for spin precession and polar motion with the solution of two decoupled models:

1. The decoupled model for polar motion can be obtained from the general model (Eq. 93) by ignoring the last four equations for the time derivative of the p-variables and by rewriting $p_{x/y}^{s/i}$ in the six first equations in terms of $m_{x/y}^{s/i}$ by means of Eq. (100). This decoupled model corresponds to Eq. (51) of Coyette et al. (2018), in which the tidal contribution should be set equal to zero.

2. As the precession is a slow motion in space, the decoupled model for spin precession can best be obtained by re-expressing the angular momentum Eqs. (54–56) in the IF. We next average the equations over the orbital period, and neglect the polar motion and longitudinal librations of the solid layers. This decoupled precession model extends the model for hydrostatic equilibrium satellite interiors (Baland et al. 2011, 2012) by including a hydrodynamic pressure (Poincaré flow). The decoupled system can be expressed as three ordinary differential equations for the projections onto the Laplace plane of the spin unit vectors of the three layers; see Eq. (176), Appendix 5.

In Sect. 3.7, we compare the free frequencies of both kinds of models. To that end, we consider two satellite toy models representative of Titan. The first model (TM1) is Titan-like, with a shell thickness of 100 km, has no surface lakes, and shares the same atmosphere dynamics as the solid toy model, but has a homogeneous interior, whereas Titan likely has an interior divided into a high-pressure ice mantle and a rocky core. The second (TM2) Titan toy model is axisymmetric and has no atmosphere. In order to investigate the case of a thick "shell", we consider a third toy model, TM3, representative of the Moon. TM3 allows easier comparison with studies about Earth rotation which includes the presence of the FOC and SIC below a thick mantle. The surface flattenings are set equal to those derived from the observed shape of Titan (see Baland et al. 2014; from Zebker et al. 2009) or of the Moon (Dumberry and Wieczorek 2016; from Araki et al. (2009)). The flattenings of the internal boundaries are chosen arbitrarily but with the condition that they decrease toward the center. For the axially symmetric TM2 and TM3, the equatorial flattenings are set to zero.

Table 5 Values for the interior parameters of two Titan (TM1 and TM2) and one Moon (TM3) Toy Models with an internal fluid layer

Parameter	TM1 (Titan-like)	TM2 (biaxial, no atmosphere)	TM3 (Moon-like)
R (km)	2575	2575	1737
R_o (km)	2475	2475	350
R_i (km)	2275	2275	200
ρ_s (km/m^3)	1000	1000	3300
ρ_o(km/m^3)	1100	1100	5800
ρ_i (km/m^3)	2250	2250	7700
α_s	19.22×10^{-5}	19.22×10^{-5}	1.29×10^{-3}
α_o	$0.8\alpha_s$	$0.8\alpha_s$	$0.8\alpha_s$
α_i	$0.6\alpha_s$	$0.6\alpha_s$	$0.6\alpha_s$
β_s	14.37×10^{-5}	0	0
β_o	$0.8\beta_s$	0	0
β_i	$0.6\beta_s$	0	0

The interior characteristics of the three toy models can be found in Table 5. In Sect. 3.8, we compare the forced solutions of coupled and decoupled rotation models, considering TM1 and the same uniform orbital precession as for the solid toy model.

3.7 Free modes for the polar motion and the precession

The frequencies σ of the free modes for polar motion and precession in the coupled model are the eigenvalues of $\mathbf{K}$, which are solutions of $\det(\sigma I_{10} - \mathbf{K}) = 0$, with I_{10} the (10×10) identity matrix. As this determinant is a polynomial of degree 5 in σ^2, we find 5 distinct free frequencies $\sigma_{CW}, \sigma_{ICW}, \sigma_{QDFWs}, \sigma_{QDFWo}$ and σ_{QDFWi} corresponding to the 5 free modes described in Table (4). Depending on the interior model considered, the free frequencies either are all real or two of them (σ_{QDFWo} and σ_{QDFWi}) are non-real complex conjugates. The toy models defined in Table 5 are characterized by real free frequencies. As in the solid case, we choose to express the frequencies as positive, and a free prograde or a free retrograde motion can be associated with each frequency, as sketched in Fig. (6). Three eigenmodes have quasi-diurnal frequency, which correspond to small frequencies $\sigma'_{FP}, \sigma'_{FON}, \sigma'_{FIN}$ in inertial space, with long periods. FP and FON modes corresponds to retrograde motions. The FIN can be prograde or retrograde, depending whether σ_{QDFWi} is smaller or larger than n. It is possible to obtain analytical expressions for the free frequencies, but since those are long and not very revealing, we focus on numerical results.

Both decoupled models are characterized by three modes: the FP, FON, and FIN for the decoupled precession model, and the CW, ICW, and FON for the decoupled polar motion (Coyette et al. 2018). The decoupled precession model does not include the CW and ICW because it does not consider the polar motion of the solid layers. The decoupled polar motion model does not consider the motion of the spin axes of the shell and of the solid interior with respect to space and as such lacks the FP and FIN. Both decoupled models have a FON mode since they both include the relative motion of the ocean rotation axis with respect to the shell.
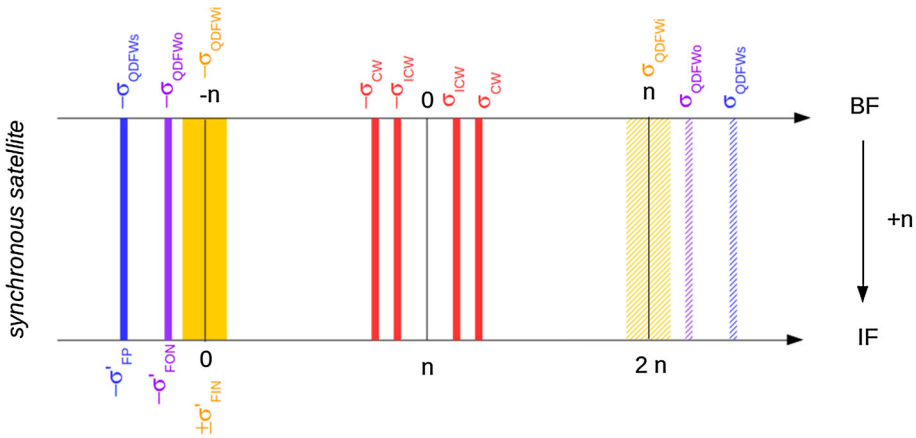
Fig. 6 Free frequencies in the body frames and in the inertial frame for a triaxial synchronous rotator with an internal global liquid ocean; see Table (4). The passage from the BF to the IF is obtained by adding the rotation rate n to the free frequencies expressed in the BF. Positive/negative frequencies correspond to prograde/retrograde motions. As in the solid case (see Fig. 1), hatched lines indicate prograde free motions which would have very small amplitudes compared to the retrograde motions at the same period

The free periods of TM1 obtained with the coupled model are gathered in Table 6 (column two). Similarly as for the CW of the solid case, the atmosphere super-rotation introduced by the term $h_z(0)$ clearly affects the periods of the CW (-34%) and of the ICW (-11%). Contrariwise, $\sigma'_{\mathrm{FP}}, \sigma'_{\mathrm{FON}}, \sigma'_{\mathrm{FIN}}$ are almost independent of $h_z(0)$ (effect $\lesssim 0.1\%$). The free periods of TM2 differ from those of TM1 due in part to the lack of atmosphere of TM2, but also to its axial symmetry, and are shorter for the CW (-16%) and ICW (-9%) and larger for the FP, FON, and FIN periods (up to $+30\%$).

We next compare the free periods of the coupled (Table 6, column 2) and decoupled (columns 3 and 4) models. For the FON, the decoupled polar motion model predicts a correct value for the Moon TM3 with its small interior, but predicts wrong values for the Titan TM1 and TM2 with their thin outer shell. This is because the decoupled polar motion model is based on the underlying assumption that the solid layers cannot have a free motion in space, which significantly alters the period of the FON when the solid interior is large. This discrepancy indicates that the decoupled polar motion model of Coyette et al. (2018) should be used with caution to predict solution at quasi-diurnal forcing periods, close to the period of the QDFW$_o$, as was noted by those authors. The agreement in the periods of the other modes between the decoupled and coupled models is good or even excellent (e.g., the difference is 6% for T_{ICW} of TM3, and 0.005% for T_{FON} of TM1).

We also compared our results for the biaxial TM2 and TM3 to well-known analytical formulae for the CW, ICW, FCN, and FICN of a biaxial Earth (e.g., page 293 of Dehant and Mathews (2015)). To do so, we first removed in **K** the terms related to the external gravitational torque and characteristics of the synchronous rotation, to get **K**$_{ns}$ (see end of Appendix 4 for the details). A good-to-excellent agreement is obtained for TM3, but the periods differ strongly for TM2 (see columns 5 and 6 of Table 6), which is due to the relatively large size of the solid interior for Titan toy models. The classical models for the rotation of the Earth assume that the solid inner core has a small moment of inertia compared to the total moment of inertia (see Sect. 5 of Mathews et al. (1991), where A_s, the equatorial moment of inertia of the SIC, is neglected in some terms of the governing equations, because of the small size of the SIC).

Table 6 Free periods (years) for the three Toy Models of Table 5

	$\mathbf{K}$ (full coupled model)	Decoupled models PM	Spin prec.	$\mathbf{K}_{ns}$ (non-synch.)	Biaxial Earth formulae
TM1					
T_{CW}	8.63 (13.06)	8.60	–	11.72	–
T_{ICW}	180.69 (202.63)	180.65	–	267.60	–
T_{FP}	9.14 (9.13)	–	9.10	16.93	–
T_{FON}	323.87 (323.87)	43.72	323.96	463.97	–
T_{FIN}	191.96 (191.95)	–	191.95	$\rightarrow \infty$	–
TM2					
T_{CW}	11.26	11.23	–	16.95	28.31
T_{ICW}	184.19	184.16	–	303.88	170.64
T_{FP}	11.00	–	10.97	18.30	–
T_{FON}	384.98	43.70	385.013	566.99	70.28
T_{FIN}	247.6	–	247.67	$\rightarrow \infty$	40.22
TM3					
T_{CW}	29.02	28.97	–	57.93	57.93
T_{ICW}	1.27	1.20	–	1.28	1.21
T_{FP}	38.68	–	38.65	$\rightarrow \infty$	–
T_{FON}	71.38	71.26	71.46	71.30	71.26
T_{FIN}	1.29	–	1.22	1.29	1.22

Column 2: free periods obtained from $\mathbf{K}$ (see Eq.93). The values in parentheses for TM1 corresponds to a case without super-rotation of the atmosphere ($h_z(0) = 0$). TM2 and TM3 have no atmosphere. Columns 3 and 4: free periods obtained from decoupled models for the polar motion (Coyette et al. 2018) and for the spin precession (see Appendix 5). Column 5: free periods obtained with a matrix $\mathbf{K}_{ns}$ where the terms related to the external torque are dropped, in order to mimic the non-synchronous case (hence the subscript ns, see end of Appendix 4). Column 6: free periods obtained for TM2 and TM3 from well-known analytical formula written originally for a biaxial Earth (see, for instance, Dehant and Mathews 2015). Values indicated in red correspond to cases where the considered model fails to provide correct periods, because of their underlying assumptions

By comparing columns 2 and 5 of Table 6, we can put further into perspective the differences between synchronous and non-synchronous rotation. For Titan TM1 or TM2, the terms in the matrix $\mathbf{K}$ of Eq. (94) related to the external gravitational torques on the solid layers, the internal gravitational torque, and the hydrodynamical torques are comprised within a range of one order of magnitude, so that neglecting the external torques significantly affects all the free periods. In particular, the CW and ICW periods are smaller due to the resonant rotation (8.6 years versus 11.7 years for CW of TM1 for instance), a behavior already observed for the CW of the solid case. As the solid interior accounts for the essential of the mass of the satellite, the FIN period tends to infinity and this mode degenerates into a TOM, juste like the FP of a solid body. For the Moon TM3, the external torque on the "shell" (which is the mantle for the Moon) largely dominates all the other torques, and is three orders of magnitude larger than the internal gravitational torque. The latter is two orders of magnitude larger than the external torque on the small solid interior. As a result, neglecting the external torques only affects the periods of the modes related to the mantle (the FP and the CW). Because of the large moment of inertia of the mantle compared to the other layers, the FP degenerates into

a TOM, and the difference between synchronous and non-synchronous rotation tends to the well-known factor 2 for the CW of an entirely solid body (Eckhardt 1981).

Besides the validation of our model through the comparisons with results from applying equations for the Earth to model TM3, we also compare our coupled model to three other rotation models. First we consider the Hamiltonian model for a satellite with a rotating internal liquid layer developed by Boué et al. (2017), and we use their Titan toy model denoted F1 for numerical comparisons. Since those authors do not consider the effect of an atmosphere, we neglect those effects in our model in the comparison. The period of the free modes obtained with our coupled model are in excellent agreement (difference $< 0.4\%$) with the ones obtained with the Hamiltonian model. We also compare the Hamiltonian model by Noyelles (2012) for the rotation of a synchronous satellite with an entirely fluid core with the outputs of our coupled model adapted to the limit case of an entirely liquid interior, for a toy model of Io with a core characterized by $\delta = C_f/C = 0.4$, or $R_f/R \simeq 0.8$. We notice an overall good match, except for the FCN period, as already noted by Boué et al. (2017), which differs by about 16%. The last comparison concerns the angular momentum coupled model of Dumberry and Wieczorek (2016) applied to the Moon. They assume that the gravitational external torque, as seen from the IF, is averaged over the Moon rotation/revolution period. The FP, FCN, and FICN, which manifest themselves in the IF at long periods, are not affected by this procedure and our results agree with their results. The CW and ICW derived from their model cannot be in agreement with those derived from our coupled model in which we use the non-averaged torque, since they have quasi-diurnal periods as seen in the IF (see Fig. 6). In the limit case of an entirely solid and axisymmetric body, the frequency σ_{CW} of Dumberry and Wieczorek (2016) turns to be $\frac{5}{2}n\frac{C-A}{A}$, instead of $2n\frac{C-A}{A}$ (see Eq. 23), the CW frequency of the solid model of Sect. 2 and of Eckhardt (1981), whereas $\sigma_{\mathrm{FP}} = \frac{3}{2}n\frac{C-A}{A}$, in agreement with our coupled model (see Eq. 25) and Eckhardt (1981).

3.8 Forced solution

The angular momentum Eq. (93) governing the coupled precession and polar motion can be solved for each frequency of the forcing **T** of Eq. (94), so that the full solution can be written, by analogy with Eq. (33) for the solid case, as

$$\mathbf{u} = \mathbf{u}_{\mathrm{ext}} + \mathbf{u}_{\mathrm{off}} + \mathbf{u}_{\mathrm{atm}}, \tag{95}$$

where the first, second, and third terms correspond to the part of the solution related to the external forcing by the parent planet, the constant terms of the atmospheric forcing, and the periodic terms of the atmospheric forcing, respectively.

In the subsections below, we discuss in details the different parts of the solution. Because the analytical solutions are too long to be written here, we only show numerical results. Figure 7 shows the evolution over one Saturn or Titan year of $\mathbf{m}_s$, $\mathbf{m}_o$, $\mathbf{m}_i$, $\mathbf{p}_s$, $\mathbf{p}_i$, θ_s, θ_o, θ_i, $\hat{s}_s$, $\hat{s}_o$, and $\hat{s}_i$ for model TM1, and Table 7 summarizes the results. We also examine the differences (presented in Fig. 8) between the coupled solution obtained here and the solutions of the decoupled models of Coyette et al. (2018) and of Appendix 5 for the polar motion and spin precession, respectively, and compare our coupled model to other published coupled models.
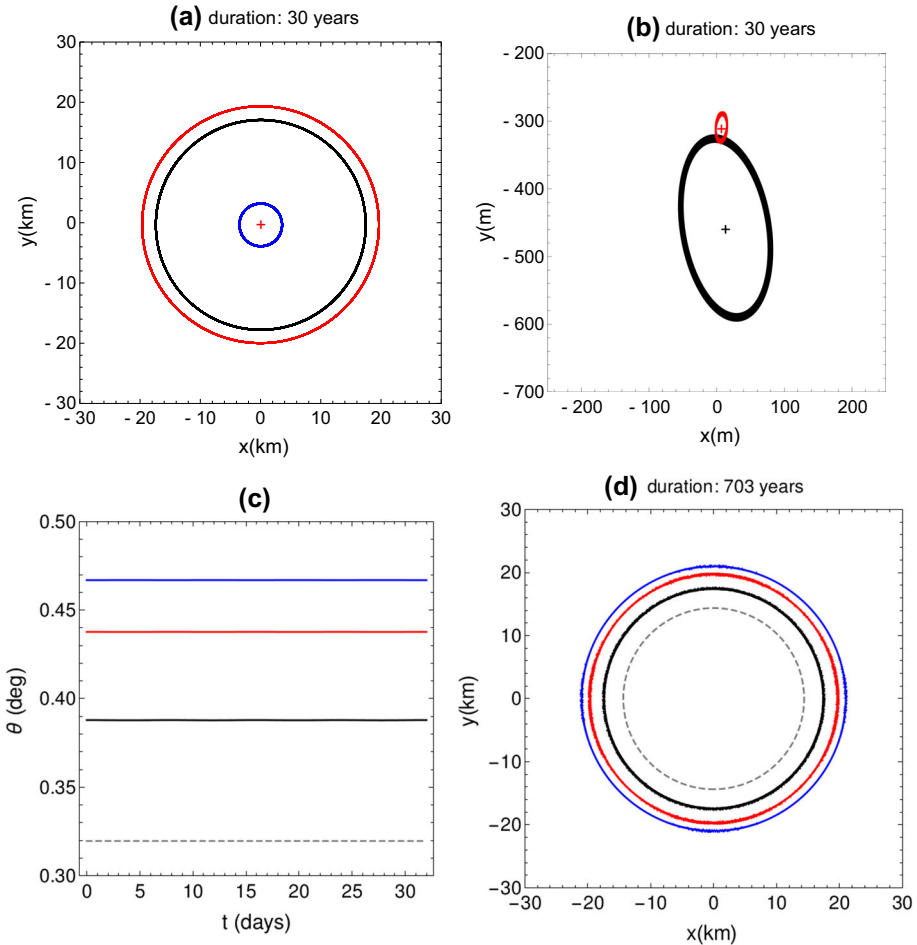
Fig. 7 Numerical solution of the system of Eq. (93) for the Titan toy model TM1 of Table 5. Panel **a** describes, as distances in kilometers at the surface of the satellite, the evolution over 30 years of the equatorial components of the unit vector along the Laplace place, both with respect to the shell BF ($\mathbf{p}_s$, black) and with respect to the interior BF ($\mathbf{p}_i$, red). The evolution of the equatorial components of the unit vector along ocean spin axis $\mathbf{m}_o$ with respect to the shell BF is presented in blue. Panel **b** describes, in meters, the evolution over 30 years of the equatorial components of the unit vector along the shell ($\mathbf{m}_s$, black) and interior ($\mathbf{m}_i$, red) spin axes, with respect to their respective BF. The evolution of $\mathbf{p}_s$, $\mathbf{p}_i$ and of $\mathbf{m}_o$ is mainly governed by the external torque, whereas the evolution of $\mathbf{m}_s$ and of $\mathbf{m}_i$ is mainly governed by the atmospheric torque. The offset due to the constant terms of the atmospheric forcing is materialized by the cross markers (black in the shell BF, red in the interior BF). Panel **c** displays the evolution over two diurnal cycles ($\simeq 32$ days) of the inertial obliquities of the shell (θ_s, black), the ocean (θ_o, blue), and of the interior (θ_i, red). The dashed gray line represents the orbital inclination, as a point of comparison. The trajectory of the unit vector along the spin axes of the three layers (same color code as for the other panels) projected onto the Laplace plane (s_x^k, s_y^k) is shown in panel **d** over the duration of the orbital precession (703 years) which drives the spin precession. The dashed gray line represents the projection of the unit vector along the orbital normal

Table 7 Amplitudes and frequencies of the different parts of the solution of Eq. (95) for the Titan TM1 of Table 5

		External torque	Atmosphere	Atmosphere
BF	Frequency	$n - \dot{\Omega}$	0	ϖ_{an}
	m_x^s	3 m	13.27 m	65 m
	m_y^s	5 m	−457.82 m	130 m
	m_x^o	3.6 km	13.27 m	65 m
	m_y^o	3.6 km	−457.82 m	130 m
	m_x^i	0.2 m	7.08 m	8 m
	m_y^i	2 m	−309.37 m	20 m
	p_x^s	17.4 km	13.27 m	65 m
	p_y^s	17.4 km	−457.82 m	130 m
	p_x^i	19.7 km	7.08 m	8 m
	p_y^i	19.7 km	−309.37 m	20 m
IF	Frequency	$\dot{\Omega}$		
	$\bar{\theta}_s$	0.388°	–	–
	$\bar{\theta}_o$	0.467°	–	–
	$\bar{\theta}_i$	0.438°	–	–
	Freq	$\simeq 2n$		$\simeq n$
	$\Delta\theta_s$	2 m	–	0.1 m
	$\Delta\theta_o$	0.25 m	–	0.00004 m
	$\Delta\theta_i$	0.5 m	–	0.001 m

The first part of the table deals with the variables **m** and **p** of the different layers, seen from the appropriate solid layer BF. The second part of the table deals with the solution expressed in the IF, and in particular with the inertial obliquities, computed as differences of the form $|\mathbf{m} - \mathbf{p}|$. Note that θ_o is computed from $|\mathbf{m}_o - \mathbf{p}_s|$, which is the sum of $\mathbf{m}_o$ and $\mathbf{p}_s$ radii (17.4 + 3.6 = 21 km, or 0.467°), as $\mathbf{m}_o$ and $\mathbf{p}_s$ are out of phase to each other by π, explaining why the ocean spin axis, as seen from the IF, is further away from the Laplace pole than the shell and interior spin axes (panel d of Fig. 7)

3.8.1 Solution related to the external forcing by the parent planet

As for the solid case, the motions induced by the external gravitational torque, at a quasi-diurnal frequency ($f = n - \dot{\Omega}$), can be separated into two categories: first, the large circular motions of several km radius ($\mathbf{p}_s$, $\mathbf{p}_i$, and $\mathbf{m}_o$, see Fig. 7, panel a), and second, the small elliptical motions of a few meters ($\mathbf{m}_s$ and $\mathbf{m}_i$, see Table 7). In addition, the external gravitational torque results in large circular motions of the rotations axes of the three layers in the IF, on the timescale of orbit precession, with quasi-constant inertial obliquities (Fig. 7, panels c and d). It also results in semi-diurnal nutations in obliquity and in longitude, at least four orders of magnitude smaller than the mean inertial obliquities (Table 7). As for the solid case, the periods of the CW (8.6 years) and of the ICW (181 years) are too far from the quasi-diurnal forcing period to produce a resonant amplification of the solution. The solution is slightly amplified though by a resonance between the forcing at 703 years and the FIN at 192 years and the FON at 324 years in inertial space. The FP has a period of about 9 years, too far from the forcing period to induce a significant amplification.

The decoupled solutions for the polar motion of the solid layers ($\mathbf{m}_{ext}^s$ and $\mathbf{m}_{ext}^i$) and for the spin precession of the three layers in space ($\hat{s}_{ext}^s$, $\hat{s}_{ext}^o$, and $\hat{s}_{ext}^i$) are taken from Coyette et al. (2018) and Appendix 5, respectively. The motion of the spin axis of the ocean, $\mathbf{m}_{ext}^o$, in the decoupled models is given by Coyette et al. (2018). An alternative decoupled solution for $\mathbf{m}_{ext}^o$ can be obtained from the decoupled precession model by injecting $\theta_0^s = i + \eta_0^s$ and $\theta_0^o = i + \eta_0^o$ into Eqs. (170–171) where the spin node longitudes ξ_s and ξ_o are set to Ω, as there are, by assumption, no nutations in the solution of the decoupled precession model. For TM1, the differences between the coupled and the decoupled solutions are below the percent level. Those small differences between the two kind of models indicate that the shell, ocean, and interior spin precession are almost decoupled from the solid layers' polar motion, because $\mathbf{m}_s$ and $\mathbf{m}_i$ are very small, compared to the Laplace pole motions. As for the solid satellite, the decoupled solution for the spin precession is accurate enough compared to the actual measurement precision of 6%.

The mean orbital obliquities are in very good agreement ($< 0.6\%$ difference) with those of Boué et al. (2017) for their model F1. Our results differ by 0.6% and 2% for the mean orbital obliquities of the mantle and fluid core, respectively, with the results of the alternative Hamiltonian model of Noyelles (2012) for an interior model of Io with a large core. Considering the Moon and the model by Dumberry and Wieczorek (2016), we obtain similar values for the tilt angles of the mantle symmetry axis with respect to the ecliptic normal. We also find that the resonant amplification with the FCN or the FICN occurs for similar values of the CMB flattening, whether the torque is averaged or not, because the FCN and FICN periods are not affected by the averaging (see Sect. 3.7). However, we find a difference of 40% in mantle polar motion, as a consequence of the torque averaging by Dumberry and Wieczorek (2016).

3.8.2 Solution related to the atmospheric forcing

Like Eckhardt's kinematic equation (12), Euler's kinematic Eq. (14) can be extended to the shell and the solid interior, explaining why for atmospheric forcing at long periods ($w \simeq 0$), we have $\mathbf{m}_{atm}^s \simeq \mathbf{p}_{atm}^s$ in the shell BF and $\mathbf{m}_{atm}^i \simeq \mathbf{p}_{atm}^i$ in the interior BF, similarly to the corresponding result for the entirely solid satellite that $\mathbf{m}_{atm} \simeq \mathbf{p}_{atm}$ (see Table 7). As the orientation of the two BF is defined with respect to the same IF, the equatorial components of the unit vector along the interior spin axis expressed in the shell BF are $\mathbf{p}_s - \mathbf{p}_i + \mathbf{m}_i$ (see Fig. 5). We find that, for $w \simeq 0$, $\mathbf{m}_{atm}^s \simeq \mathbf{m}_{atm}^o \simeq \mathbf{p}_{atm}^s - \mathbf{p}_{atm}^i + \mathbf{m}_{atm}^i$, meaning that the three rotation axes would be almost aligned if there were no other torques than the torque exerted by the atmosphere at long periods (see Fig. 9). This is expected since the periods of the FP (9 years), FON (324 years), and FIN (192 years) are larger than the forcing period as seen from the IF (quasi-diurnal), so that none of the spin axes is able to follow the forcing in the IF and they tend to keep a fixed orientation, along the Laplace pole. At the same time, in the BF's, the spin axis of each solid layer reaches an equilibrium orientation which reflects the balance between the orientation of the atmospheric angular momentum and the orientation of the layer's principal polar axis of inertia. As the internal gravitational and pressure torques are too weak to restore the alignment between the two BF's, $\mathbf{p}_{atm}^s - \mathbf{p}_{atm}^i \neq 0$.

For TM1, the polar offsets ($w = 0$) are a few hundred meters (see Table 7) and are in near perfect agreement (difference $< 0.0001\%$) with the values derived from Eq. (61–66) of Coyette et al. (2018). The annual solution ($w = \varpi_{an}$) consists of ellipses of a few tens to a few hundreds meters, as can be seen in panel (b) of Fig. (7). $\mathbf{m}_{atm}^s$ and $\mathbf{m}_{atm}^i$ are larger than $\mathbf{m}_{ext}^s$ and $\mathbf{m}_{ext}^i$, whereas $\mathbf{p}_{atm}^s$, $\mathbf{p}_{atm}^i$ and $\mathbf{m}_{atm}^o$ are surpassed by the quasi-diurnal solutions $\mathbf{p}_{ext}^s$, $\mathbf{p}_{ext}^i$ and $\mathbf{m}_{ext}^o$ related to the torque exerted by the parent planet. The annual solution
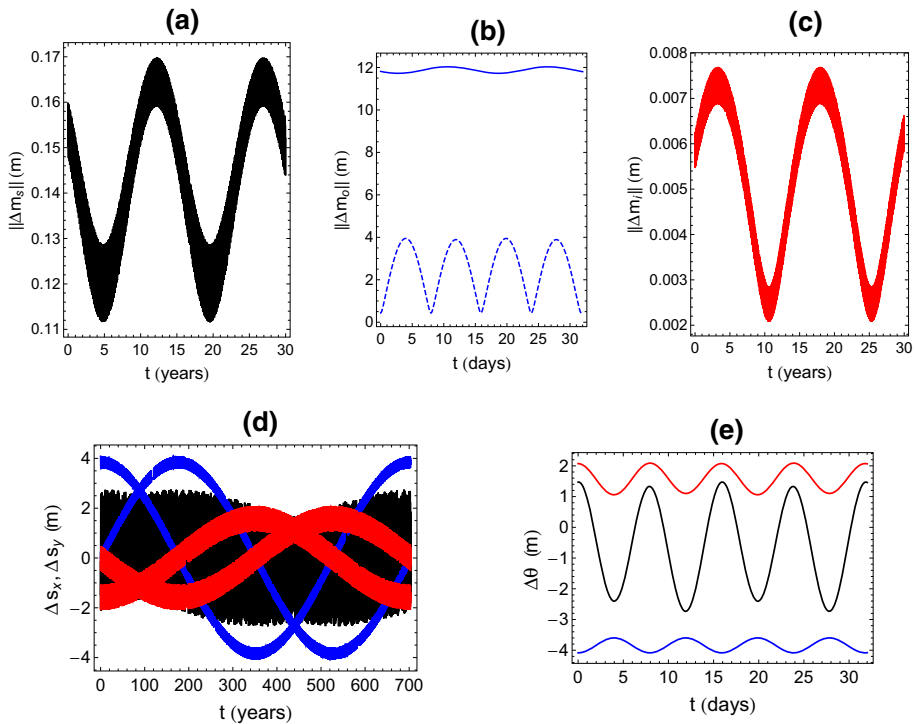
Fig. 8 Panels **a**, **b**, **c**: Differences, as distances in meters at the surface of Titan, between the numerical solution of the coupled system of Eq. (93) and the analytical solutions of the decoupled models for the amplitude of $\mathbf{m}_s$, $\mathbf{m}_o$, and $\mathbf{m}_i$. For the solid layers, the decoupled model is the one of Coyette et al. (2018). For the ocean, the decoupled model can either be the one of Coyette et al. (2018), see the solid line, or the one obtained from the decoupled spin precession solution and Eqs. (170–171), see the dashed line. The difference between the coupled model and the decoupled model of Coyette et al. (2018) for $\mathbf{m}^s_{\mathrm{ext}}$, $\mathbf{m}^o_{\mathrm{ext}}$ and $\mathbf{m}^i_{\mathrm{ext}}$ results in the small diurnal oscillations in panels a, b, and c. The larger oscillations in panel a and c correspond to the differences for $\mathbf{m}^s_{\mathrm{atm}}$ and $\mathbf{m}^i_{\mathrm{atm}}$, at annual period. Panel (d) represents the differences in projected unit spin vectors onto the Laplace plane (black for the shell, blue for the ocean, and red for the interior). Panel (e) is for the differences in inertial obliquities between the numerical coupled solution and the analytical decoupled solution derived from Eq. (182). The differences between the coupled and the decoupled spin precession models in mean obliquities correspond to the amplitude of the oscillations that occur at the 703-year period in panel d and to the mean values of the curves of panel e. The differences in $\mathbf{m}^o_{\mathrm{ext}}$ and in nutations driven by the external gravitational torque (which are zero in the decoupled spin precession model) manifest themselves as the small semi-diurnal oscillations in panels b, d and e. The nutations in space related to the atmospheric torque are so small (see Table 7) that their effect cannot be seen here

obtained here for the polar motion of the solid layers is in agreement to better than 1% with the annual decoupled solutions of Coyette et al. (2018) (see Fig. 8). As a consequence of the Euler equation (14), the polar offset does not contribute to the inertial obliquities θ_k and to the spin precession vectors $\hat{s}_k$, whereas the contribution of the annual solution is very small (see Table 7).

Resonant amplification of polar motions and Laplace pole motions to the km level is possible for forcing periods close to $2\pi/\sigma_{\mathrm{CW}} \simeq 9$ years. It is also possible in principle for forcing periods close to $2\pi/\sigma_{\mathrm{ICW}} \simeq 181$ years, however, such large forcing periods are not likely to exist. The polar motion and Laplace pole resonant amplification by the CW do not result in a significant amplification of the nutations, as the three spin axes tend to stay fixed
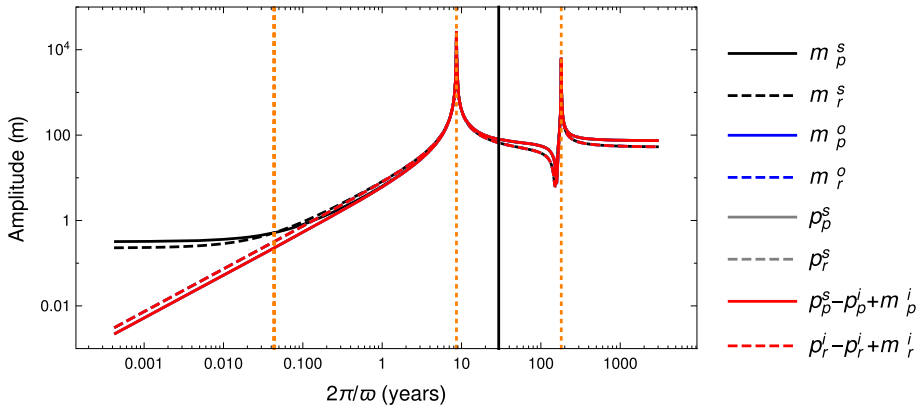
Fig. 9 Amplitudes of the atmosphere contribution to the prograde and retrograde parts of the solution for the PM and Laplace pole motion, as a function of the forcing period, assuming that the forcing amplitudes at any period are those of the annual forcing. The solid vertical black line indicates the annual period of the atmospheric forcing. The dashed orange lines are, from left to right, the three QDFW (which cannot be distinguished from each other here), CW, and ICW periods. Blue (ocean spin axis), gray (Laplace pole) and red (interior spin axis, seen from the shell BF) lines cannot be distinguished from each other

in space at long periods, as explained above. For atmospheric forcings at shorter periods, polar motions and Laplace pole motion would differ more from each other (see Fig. 9), but the amplitudes of the motions would be so small that the corresponding nutations can be neglected as well. Resonant amplifications to the km level are unlikely for forcing frequencies close to $\sigma_{\text{QDFWs,o,i}}$ because it would require a very good match between frequencies, and no attenuation by dissipative processes.

4 Discussion and conclusions

We have developed a model for the rotation of synchronously rotating satellites (e.g., Titan) in an angular momentum approach that treats in a consistent way the polar motion and the spin precession, which are kinematically coupled to each other. We have assessed the validity of assumptions usually made in decoupled models that break the link between the two motions, by comparing the results from the decoupled models with the fully coupled model. Assessing the accuracy of the decoupled models is important, because they have practical analytical solutions which can easily be used to interpret observations from past and future space missions. In addition, we have evaluated the rotation variations that have not been considered in the decoupled cases, such as, the effect of an atmosphere on the spin precession/nutation.

As Eckhardt (1981) showed, a solid synchronously rotating satellite in the Cassini state has two free modes of librations in latitude in the BF, a long-period one and a quasi-diurnal one, that we call here Chandler Wobble (CW) and Quasi-Diurnal Free Wobble (QDFW), respectively. The QDFW translates into a long period Free Precession (FP) in the IF and degenerates into a Tilt-Over Mode for the Earth (Smith 1977). The CW is named after the Earth's Chandler Wobble, but its period is about half that expected for a non-synchronously body like the Earth because of the gravitational torque of the central body, in case that the satellite has no super-rotating atmosphere. Titan's atmosphere significantly further shortens

the CW period (Coyette et al. 2016). In the CW mode, the orientation of the spin axis differs from the orientation of the pole of the BF, but the spin axis remains essentially fixed in space. In contrast, in the QDFW mode, the spin axis remains essentially fixed with respect to the BF but moves with respect to the Laplace pole. The free polar motion and free precession are then almost decoupled from each other, and the free modes of the decoupled models of Coyette et al. (2016) and Baland et al. (2011) for a solid and rigid synchronous satellite are good approximations of the free modes of the coupled model. We showed that Titan's super-rotating atmosphere only marginally affects the FP period.

We have extended the model to the presence of an internal global liquid ocean and have chosen to introduce a set of rotation variables that differs from the one of Mathews et al. (1991), introduced for the Earth, for two reasons. First, it allows for a more intuitive identification between the variables and the free modes associated with them, especially for the ICW. Second, it facilitates the comparison with existing decoupled rotation models. Each BF is oriented with respect to the IF by one rotation variable, instead of being oriented only with respect to each other. The polar motion of the interior is defined with respect to its own BF, and the motion of the ocean spin axis is directly defined with respect to the shell BF, instead of being defined with respect to the shell spin axis. We have identified five latitudinal free modes, namely the long-period Chandler Wobble (CW) and Interior Chandler Wobble (ICW), and the Quasi-Diurnal Free Wobbles of the shell (QDFWs), ocean (QDFWo), and interior (QDFWi). The three quasi-diurnal modes translates into a long period shell Free Precession (FP), a Free Ocean Nutation (FON), and a Free Interior Nutation (FIN) in the IF. The QDFWo/FON is the analog of the NDFW (Nearly diurnal Free Wobble)/FCN (Free Core Nutation) of the non-synchronous Earth, whereas the FIN replaces the FICN (Free Inner Core Nutation), also called PFCN (Prograde Free Core Nutation). We showed that the free precession and nutations are not significantly affected by the presence of the super-rotating atmosphere. For a synchronous rotation, the FIN can be prograde or retrograde, depending on the details of the internal structure. The decoupled precession model performs well in reproducing the FP, FON, and FIN modes of the coupled model. The decoupled polar motion model performs well in reproducing the CW and ICW modes of the coupled model, but not in reproducing the FON, as a consequence of the assumption in that model that the spin precession of the solid layers are already know motions. We have compared our results with those of the Hamiltonian model by Boué et al. (2017) for Titan, which neglects the atmosphere, and obtained excellent agreement with differences smaller than 0.4%.

We have shown that the spin precession, both for the solid and ocean cases, is mainly governed by the external torque. The motion in space of the spin axis of the solid satellite or of a given layer nearly follows a cone whose aperture (or mean inertial obliquity) is the sum of the orbital inclination and of the mean orbital obliquity. The mean orbital obliquity slightly differs ($+0.1\%$, for Titan in the solid case) from the one predicted by a decoupled model, as a result of a very weak coupling with polar motion. Superimposed on these precession motions, which have a period equal to that of the orbital precession, there are small semi-diurnal and diurnal nutations ($\pm 0.01\%$ in the solid case), also arising from the coupling with polar motion, and mainly due to the external torque, but also, to a lesser extent, to the atmospheric torque. As the actual precision of the measurement of Titan's obliquity is of 6% (Meriggiola et al. 2016), we conclude that the analytical solutions of the decoupled spin precession models of Baland et al. (2011) and of Sect. 5 for the solid and ocean cases, respectively, are very good approximations.

The polar motion of a solid rigid satellite, or of the shell in the ocean case, reaches a few hundred meters and is mainly governed by the atmospheric torque. The spin axis trajectory at Titan's surface is an ellipse traveled with the annual period and whose center is offset from the

figure axis of the BF because of the constant term of the atmospheric forcing. The amplitude of the annual interior polar motion is about one order of magnitude smaller than for the shell polar motion. Small quasi-diurnal variations of a few meters amplitude are superimposed onto the elliptical motions due to the weak coupling with the spin precession. As the effect of the external torque on polar motion is small, the solution of the decoupled polar motion of Coyette et al. (2016, 2018) for the solid and ocean cases, respectively, where the orbital obliquities are replaced by the solutions of Baland et al. (2011) or of Sect. 5, are very good approximations. When considering atmospheric forcing at a period close to the CW period (about 9 years for the Titan toy model with an ocean considered), it would be possible to trigger a resonant amplification of the shell polar motion to the detection level (1 km).

Besides applying our formalism to the case of icy satellites with a relatively thin outer shell (e.g., Titan), we also considered satellites with a large outer mantle (e.g., the Moon) and the limit case of our equations for non-synchronous bodies (e.g., Earth), in order to further validate our results. We have found a good match with free modes computed from the classical relations originally written for the Earth. This partially validates our models, but also reminds us that Earth formula have an application domain restricted to the case of bodies with a thick outer layer. We also consider the Moon in view of a comparison with a similar study based on the formalism developed by Mathews et al. (1991) for the Earth. We have reached agreement with the angular momentum model of Dumberry and Wieczorek (2016), but only for the part of the solution related to the precession in space. Because the external torque they used has been averaged over short period in IF, the part of their solution related to the polar motion cannot be used for validation or prediction.

In our method, we considered all solid layers to be rigid. Tidal deformations, for a large satellite like Titan, significantly affects the decoupled solutions (Coyette et al. 2016; Baland et al. 2016), but we do not expect them to enhance the coupling between polar motion and precession to a point where the decoupled solutions would be inaccurate enough to prevent measurement interpretation and predictions.

1 Appendix 1: Cassini state and orientation of the different layers

Let i and θ be the orbital inclination and inertial obliquity of a solid synchronous satellite, and χ, ϵ and ϕ the Euler angles between the rotation reference frame and the Body Frame (see Fig. 10). As can be seen from Fig. 10, since i, θ and ϵ are small angles, the synchronous rotation implies that (e.g., Peale 1969)

$$\chi + \phi + \xi - \gamma \simeq \Omega + \omega - \pi + \nu - s, \tag{96}$$

where Ω and ξ are the longitudes of the ascending nodes of the orbital plane and of the equator of the rotation frame over the inertial plane, ω is the orbit pericenter node, ν is the true anomaly ($\nu = M + s$ with M the mean anomaly and $s = 2e \sin M$ the equation of the center), and γ is the libration angle. Assuming that the synchronous satellite is in a Cassini state, the spin axis, the normal to the orbit and the normal to the Laplace/inertial plane are
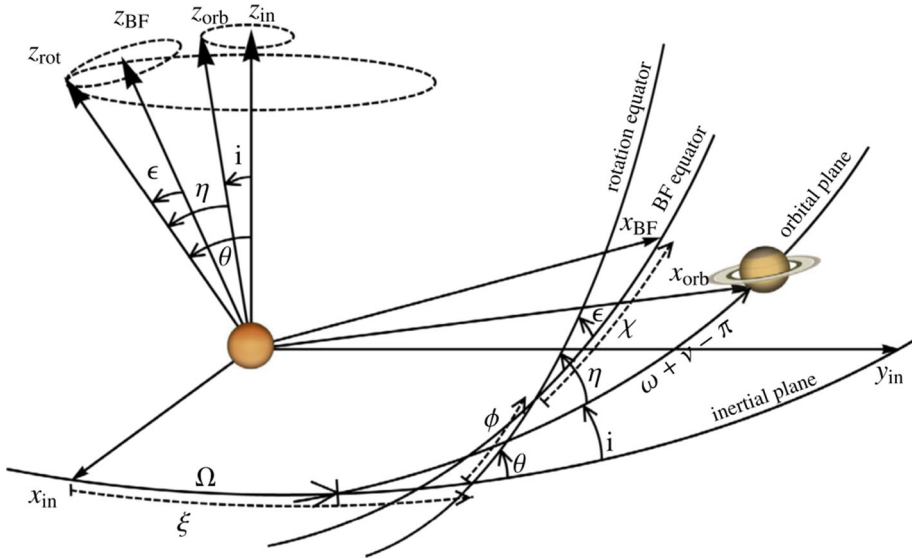
Fig. 10 From Coyette et al. (2016). Angles between the inertial plane, the orbital plane, the BF equator, and the rotation equator for a solid satellite. The angle definitions also apply to any solid layer of a satellite with an internal liquid layer. For the ocean, we have chosen not to define a Body Frame, but the rotation frame is well defined

nearly coplanar, so that

$$\xi = \Omega + \sigma, \tag{97}$$

$$\theta \simeq i + \eta, \tag{98}$$

with σ a small difference between the two node longitudes and η the orbital obliquity. The definition of the polar motion implies that

$$(m_x, m_y) \simeq -\epsilon \, (\sin \chi, \cos \chi), \tag{99}$$

with m_x and m_y the equatorial components of the rotation normalized rotation vector of Eq. (1).

Following Eckhardt (1981), we define a unit vector $\hat{p} = (p_x, p_y, p_z)$ from the satellite center, along the direction of the Laplace/inertial pole (see Eq. 6). Taking advantage of the angles defined above, its components in the BF can be written, at first order in small quantities, as

$$\hat{p} = Rz[\chi].Rx[-\epsilon].R_z[\phi].R_x[\theta]. \begin{pmatrix} 0 \\ 0 \\ 1 \end{pmatrix} \simeq \begin{pmatrix} m_x - \theta \sin(M + \omega) \\ m_y - \theta \cos(M + \omega) \\ 1 \end{pmatrix} \tag{100}$$

and expresses the motion of the Laplace pole with respect to the body frame as a combination of the polar motion of the rotation axis in the BF and of the precession of the rotation axis in space with amplitude θ. Since the difference between $\hat{p}$ (Laplace pole motion with respect to BF) and $\boldsymbol{\Omega}$ (spin axis with respect to BF, see Eq. (1)) describes the difference between Laplace and spin poles, the inertial obliquity θ is simply computed, from p_x, p_y, m_x, m_y, as:

$$\theta \simeq \sqrt{(p_x - m_x)^2 + (p_y - m_y)^2}. \tag{101}$$

The components of the unit vector $\hat{s} = (s_x, s_y, s_z)$ along the direction of the rotation axis, expressed in the Cartesian coordinates of the Laplace/inertial reference frame are given, at first order in θ, by

$$\hat{s} = Rz[-\xi].R_x[-\theta].\begin{pmatrix} 0 \\ 0 \\ 1 \end{pmatrix} \simeq \begin{pmatrix} \theta \sin(\xi) \\ -\theta \cos(\xi) \\ 1 \end{pmatrix} \tag{102}$$

and expresses the precession of the rotation axis in space, with amplitude θ. The precession is slightly influenced by the polar motion through θ, as can be seen from Eq. (101). The effect is about 5 m for the Titan toy model (see Sect. 2.4.3). The spin precession is also slightly influenced by the librations/LOD variations through ξ. The angle ξ can be extracted from Eq. (96), where ϕ can be obtained from spheric trigonometry relations (the triangle formed by the ascending node of the rotation equator over the BF equator, the descending node of the Laplace plane over the BF equator and the ascending node of the rotation equator over the Laplace plane is fully determined by the knowledge of **m** and **p**) and where γ can be replaced by the solutions of Van Hoolst et al. (2009) for libration and semi-annual LOD variations, for example. The effect of γ on the precession (not shown here) is a few meters, and can be safely neglected in front of the 1-km detection limit related to the position error of Cassini radar images (Meriggiola et al. 2016).

The unit vector **n** along the direction of the orbit pole expressed in the Cartesian coordinates of the Laplace/inertial reference frame is given, at first order in i, by

$$\hat{n} = Rz[-\Omega].R_x[-i].\begin{pmatrix} 0 \\ 0 \\ 1 \end{pmatrix} \simeq \begin{pmatrix} i \sin(\Omega) \\ -i \cos(\Omega) \\ 1 \end{pmatrix} \tag{103}$$

and the exact expression for the orbital obliquity η of Eq. (98) is given by

$$\cos \eta = \hat{n}.\hat{s}. \tag{104}$$

The definitions of and the relations between the angles presented above also apply to any solid layer of a satellite with an internal liquid layer. We simply add a subscript or superscript to indicate to which layer each quantity is related. For instance, the inertial obliquity of Titan's shell and interior are expressed as

$$\theta_s \simeq \sqrt{(p_x^s - m_x^s)^2 + (p_y^s - m_y^s)^2}, \tag{105}$$

$$\theta_i \simeq \sqrt{(p_x^i - m_x^i)^2 + (p_y^i - m_y^i)^2}. \tag{106}$$

As the orientation of the ocean masses depends on the orientation of the adjacent solid layers, which are misaligned to each other, we have chosen not to define a Body Frame for the ocean. However, the definition of an ocean rotation frame still stands. For instance, the inertial obliquity of Titan's ocean is expressed as

$$\theta_o \simeq \sqrt{(p_x^s - m_x^o)^2 + (p_y^s - m_y^o)^2}. \tag{107}$$

In both the solid and ocean cases, we have chosen to work with unit vector(s) from the satellite (solid layers) center, along the direction of the Laplace/inertial pole (see Eq. 6), as variables to be solved for, in order to properly take into account the coupling between polar motion and spin precession. This has consequences for some expressions (torques, transformation matrix) defined in the decoupled models of polar motion by Coyette et al. (2016,2018) where the spin precession was assumed to be known. These modifications are explained in the subsections below.

1.1 Consequence on the transformation matrix

The transformation matrix $R_{(i\to s)}$ from the interior BF to the shell BF is a composition of rotations, as detailed in Coyette et al. (2016). Adapting their Eq. (119) to our set of variables to be solved for in the ocean case of Sect. 3, and using relations of the form of Eq. (100) written for the two solid layers, the transformation matrix can be expressed as

$$R_{(i\to s)} = \begin{pmatrix} 1 & (\gamma_s - \gamma_i) & (p_x^s - p_x^i) \\ (\gamma_i - \gamma_s) & 1 & (p_y^s - p_y^i) \\ (p_x^i - p_x^s) & (p_y^i - p_y^s) & 1 \end{pmatrix}. \tag{108}$$

1.2 Consequence on the external and internal gravitational torques

Adapting Eq. (18) of Coyette et al. (2016) for the external torque on a solid body to our set of variables to be solved in the solid case, we easily obtain Eq. (5).

For the ocean case, the external torques on the solid layers, corrected for the effect of the hydrostatic pressure of Eqs. (85–86) become

$$\mathbf{\Gamma}_{s,\widetilde{\text{ext}}}^s = 3n^2 \begin{pmatrix} 0 \\ [(A_s - C_s) + (A_{ot} - C_{ot})][i\sin(\omega + M - \pi) - p_x^s] \\ [(B_s - A_s) + (B_{ot} - A_{ot})](s - \gamma_s) \end{pmatrix}, \tag{109}$$

$$\mathbf{\Gamma}_{i,\widetilde{\text{ext}}}^s = 3n^2 \begin{pmatrix} 0 \\ [(A_i - C_i) + (A_{ob} - C_{ob})][i\sin(\omega + M - \pi) - p_x^i] \\ [(B_i - A_i) + (B_{ob} - A_{ob})](s - \gamma_i) \end{pmatrix}, \tag{110}$$

whereas Eqs. (124–129) of Coyette et al. (2016) for the internal gravitational torque between the solid layers, here corrected for the effect of the hydrostatic pressure of Eqs. (85–86), become:

$$\mathbf{\Gamma}_{\widetilde{int}}^s = \begin{pmatrix} -n\kappa_{\text{int}}^x (p_y^s - p_y^i) \\ n\kappa_{\text{int}}^y (p_x^s - p_x^i) \\ n\kappa_{\text{int}}^z (\gamma_s - \gamma_i) \end{pmatrix} = -\mathbf{\Gamma}_{\widetilde{int}}^i, \tag{111}$$

with

$$\kappa_{\text{int}}^x = \frac{4\pi G}{5n}(C_i - B_i + C_{ob} - B_{ob})(\rho_s[2(\alpha_s - \alpha_o) - (\beta_s - \beta_o)] + \rho_o(2\alpha_o - \beta_o)), \tag{112}$$

$$\kappa_{\text{int}}^y = \frac{4\pi G}{5n}(C_i - A_i + C_{ob} - A_{ob})(\rho_s[2(\alpha_s - \alpha_o) + (\beta_s - \beta_o)] + \rho_o(2\alpha_o + \beta_o)), \tag{113}$$

$$\kappa_{\text{int}}^z = -\frac{8\pi G}{5n}(B_i - A_i + B_{ob} - A_{ob})(\rho_s(\beta_s - \beta_o) + \rho_o\beta_o). \tag{114}$$

2 Appendix 2: A coupled system for a solid axisymmetric non-synchronous planet

Consider a non-synchronous planet rotating at the mean rate Ω_o, different from its revolution rate n, so that its rotation vector is written as

$$\boldsymbol{\Omega} = \Omega_o \begin{pmatrix} 0 \\ 0 \\ 1 \end{pmatrix} + \Omega_o \, \mathbf{m} = \Omega_o \begin{pmatrix} m_x \\ m_y \\ 1 + m_z \end{pmatrix}, \tag{115}$$

instead of Eq. (1) for the synchronous case. Neglecting librations (since we assume $A = B$) and assuming that the obliquity θ is a small angle (this assumption is not justified for planets like the Earth with a large obliquity, but is practical in the following), Eq. (96) is replaced by

$$\chi + \phi + \xi \simeq \Omega_o t. \tag{116}$$

For simplicity, we have assumed that the phase of $\chi + \phi + \xi$ is zero at $t = 0$. We also assume that the orbit is circular ($e = 0$), that the orbital plane is the inertial plane ($i = 0$), so that $\Omega + \omega + M = L$ with L the mean longitude defined as $nt + L_o$.

Equation (99) for polar motion in the BF also applies in the non-synchronous case, whereas Eq. (100) for the Laplace pole motion changes to

$$\hat{p} \simeq \begin{pmatrix} m_x - \theta \sin(\Omega_o t - \xi) \\ m_y - \theta \cos(\Omega_o t - \xi) \\ 1 \end{pmatrix}. \tag{117}$$

As a result, the components of the unit vector in the direction to the Sun in the coordinates of the planet BF can be written as

$$\begin{pmatrix} r_x \\ r_y \\ r_z \end{pmatrix} = \begin{pmatrix} -\cos(L - \Omega_o t) \\ -\sin(L - \Omega_o t) \\ p_x \cos(L - \Omega_o t) + p_y \sin(L - \Omega_o t) \end{pmatrix} \tag{118}$$

and the components of the torque exerted by the Sun are given by

$$\boldsymbol{\Gamma}_{\mathrm{pb}} = \frac{3}{2} n^2 (C - A) \begin{pmatrix} -p_y + p_y \cos 2(L - \Omega_o t) - p_x \sin 2(L - \Omega_o t) \\ p_x + p_x \cos 2(L - \Omega_o t) + p_y \cos 2(L - \Omega_o t) \\ 0 \end{pmatrix}. \tag{119}$$

By dropping the terms of the torque which explicitly depend on the forcing frequency $2(n - \Omega_o)$, the homogeneous system, formed by the angular momentum equation and the kinematic equation, to be solved to find the free latitudinal modes is written as

$$A\Omega_o \dot{m}_x + (C - A)\Omega_o^2 m_y = -\frac{3}{2} n^2 (C - A) p_y, \tag{120}$$

$$A\Omega_o \dot{m}_y - (C - A)\Omega_o^2 m_x = \frac{3}{2} n^2 (C - A) p_x, \tag{121}$$

$$\dot{p}_x = \Omega_o p_y - \Omega_o m_y, \tag{122}$$

$$\dot{p}_y = -\Omega_o p_x + \Omega_o m_x, \tag{123}$$

and is characterized by the following frequencies

$$\sigma_{\mathrm{CW}} = \frac{3n^2 + 2\Omega_o^2}{2\Omega_o} \frac{(C - A)}{A}, \tag{124}$$

$$\sigma_{\text{QDFW}} = \frac{3n^2}{2\Omega_o} \frac{(C-A)}{A} + \Omega_o. \tag{125}$$

The main difference with respect to the homogeneous part of the system of Eqs. (15–18), besides the neglect of the atmosphere, is the existence of a term in p_y in Eq. (120) and the modification of the right-hand side in the y-component of the angular momentum Eq. (121) by a factor $1/2$.

Our expression for σ_{CW} slightly differs from the classical expression (see below) derived from a decoupled system for polar motion. In the IF, the QDFW translates to a free precession with

$$\sigma'_{\text{FP}} = \frac{3n^2}{2\Omega_o} \frac{(C-A)}{A}, \tag{126}$$

similar to the classical expression for the precession rate of a non-synchronous planet, as derived from a decoupled equation for the spin precession in space (see below, Eq. 131), but without the factor $\cos\theta_o$, with θ_o the mean obliquity, as we have assumed that $\theta \ll 1$.

In studies dealing with the rotation of the Earth, it is customary to neglect the torque to find the free modes (e.g., page 47 of Moritz and Mueller (1987)). In that case, the angular momentum equation governing the Chandler Wobble can be solved independently from the kinematic equation, and the CW frequency reduces to the classical expression

$$\sigma_{\text{CW}} = \Omega_o \frac{(C-A)}{A}. \tag{127}$$

The CW is a purely prograde (see Eq. 2.10a of Smith (1977)) mode of **m**. The effect of the external torque on the CW, obtained as the difference between Eq. (124) and Eq. (127), is only 0.001% for the Earth, since $n \ll \Omega_o$, and can safely be neglected.

Still neglecting the torque, but considering both the angular momentum and kinematic equations (note that the concept of *kinematic equation* here plays the same role as the concept of *nutation frame* introduced in Sect. 2.3.1 of Moritz and Mueller (1987), that is to say orienting the BF with respect to the IF), we also obtain the QDFW and FP frequencies which are given by

$$\sigma_{\text{QDFW}} = \Omega_o, \tag{128}$$
$$\sigma'_{\text{FP}} = 0. \tag{129}$$

The QDFW is a purely retrograde (and diurnal) mode of **p**. We see that when the external torque is neglected, the Free Precession degenerates into a mode called the Tilt-Over mode (TOM) and where the spin axis stays fixed in space. However, it is very well known that the Earth is precessing in space with a finite period (about 26, 000 years). The TOM and its infinite period is therefore not strictly speaking an existing rotation mode, but a mathematical degeneracy due to an extreme approximation ($n \ll \Omega_o$) when dealing with equations written in the BF.

It is possible to write an angular momentum for the precession in the IF, by neglecting polar motion (see, e.g., Eq. (1) of Bills (2005)):

$$\frac{d\hat{s}}{dt} = \frac{1}{(1-e^2)^{3/2}} \frac{3}{2} \frac{C-A}{C} \frac{n^2}{\Omega_o} (\hat{n}.\hat{s})(\hat{s} \wedge \hat{n}). \tag{130}$$

Relaxing the assumption that the mean obliquity θ_o is a small angle, $\hat{s} = (s_x, s_y, s_z \simeq \cos\theta_o)$ and $\hat{n} = (n_x, n_y, n_z \simeq 1)$. The free frequency associated to Eq. (130), obtained by setting

$n_x = n_y = 0$ (or $i = 0$) is

$$\sigma'_{\text{FP}} = \frac{1}{(1 - e^2)^{3/2}} \frac{3n^2}{2\Omega_o} \cos\theta_o \frac{(C - A)}{A},$$ (131)

which is a generalization of Eq. (126) to an eccentric orbit and large obliquity.

The considerations above question the very definition of what is a free mode. Is it the solution obtained when the whole torque is neglected? Or is it the solution of the homogeneous system of equations? For the Earth, it is customary to assume that the homogeneous system of equations is indeed obtained by neglecting the torque. However, we have seen above that this is not entirely justified. For synchronous rotators in the Cassini state, the dependence of the torque on the orientation of the BF with respect to the IF is clearly apparent (see Eq. 5), and it is easy to understand how the torque affects the homogeneous system. For the Earth, it is not customary to attempt to write the torque as a function of the variable to be solved for, and the effect of the torque on the homogeneous system is usually overlooked.

3 Appendix 3: Solution for the periodic atmospheric coupling, in the solid rigid case

The solution corresponding to the periodic terms of the atmospheric forcing of Eq. (8) is given, by

$$\begin{pmatrix} m_x \\ m_y \\ p_x \\ p_y \end{pmatrix}_{\text{atm}} \simeq \sum_{\varpi \neq 0} \begin{pmatrix} m_y^s(\varpi) \sin(\varpi t + \phi_y(\varpi)) + m_x^c(\varpi) \cos(\varpi t + \phi_x(\varpi)) \\ m_y^c(\varpi) \cos(\varpi t + \phi_y(\varpi)) + m_x^s(\varpi) \sin(\varpi t + \phi_x(\varpi)) \\ p_y^s(\varpi) \sin(\varpi t + \phi_y(\varpi)) + p_x^c(\varpi) \cos(\varpi t + \phi_x(\varpi)) \\ p_y^c(\varpi) \cos(\varpi t + \phi_y(\varpi)) + p_x^s(\varpi) \sin(\varpi t + \phi_x(\varpi)) \end{pmatrix},$$ (132)

where

$$m_y^s(\varpi) = \upsilon_y \left(n^2 \varpi \left(-\frac{h_z(0)}{n} + (4A + B - 6C) \right) \right.$$
$$\left. + \varpi^3 \left(\frac{h_z(0)}{n} - (A + B - 3C) \right) \right),$$

$$m_y^c(\varpi) = \upsilon_y \left(n^3 \left(\frac{h_z(0)}{n} + 4(-A + C) \right) \right.$$
$$\left. + n\varpi^2 \left(-\frac{h_z(0)}{n} + (A - B + C) \right) + \frac{\varpi^4}{n}(B - 2C) \right),$$

$$m_x^c(\varpi) = \upsilon_x \left(n^3 \left(\frac{h_z(0)}{n} + (-B + C) \right) \right.$$
$$\left. + n\varpi^2 \left(-\frac{h_z(0)}{n} + (-4A + B + 4C) \right) + \frac{\varpi^4}{n}(A - 2C) \right),$$

$$m_x^s(\varpi) = \upsilon_x \left(n^2 \varpi \left(\frac{h_z(0)}{n} - (4A + B - 6C) \right) \right.$$
$$\left. + \varpi^3 \left(-\frac{h_z(0)}{n} + (A + B - 3C) \right) \right),$$

$$p_y^s(\varpi) = \upsilon_y (n^2 - \varpi^2)\varpi (B - 2C),$$

$$p_y^c(\varpi) = \upsilon_y \left(n^3 \left(\frac{h_z(0)}{n} + 4(-A + C) \right) - n\varpi^2 \left(\frac{h_z(0)}{n} + (-A + C) \right) \right),$$

$$p_x^c(\varpi) = \upsilon_x \left(n^2 - \varpi^2 \right) n \left(\frac{h_z(0)}{n} + (-B + C) \right),$$

$$p_x^s(\varpi) = \upsilon_x \left(n^2 \varpi (-4A + 5C) + \varpi^3 (A - 2C) \right),$$

$$\upsilon_x = \frac{h_x(\varpi)}{C^2(\varpi^2 - \sigma_{CW}^2)(\varpi^2 - \sigma_{QDFW}^2)},$$

$$\upsilon_y = \frac{h_y(\varpi)}{C^2(\varpi^2 - \sigma_{CW}^2)(\varpi^2 - \sigma_{QDFW}^2)}.$$

For $\varpi \to 0$, $(m_y^s, m_x^s, p_y^s, p_x^s) \to 0$ and $(m_y^c, m_x^c) \to (p_y^c, p_x^c)$, so that $(m_x^{atm}, m_y^{atm}) \simeq (p_x^{atm}, p_y^{atm})$.

The solution can also be written in elliptical form

$$\begin{pmatrix} m_x \\ m_y \\ p_x \\ p_y \end{pmatrix}_{atm} \simeq \sum_{\varpi \neq 0} \begin{pmatrix} \tilde{m}_x(\varpi) \sin(\varpi t + \tilde{\phi}_x(\varpi)) \\ \tilde{m}_y(\varpi) \cos(\varpi t + \tilde{\phi}_y(\varpi)) \\ \tilde{p}_x(\varpi) \sin(\varpi t + \tilde{\varphi}_x(\varpi)) \\ \tilde{p}_y(\varpi) \cos(\varpi t + \tilde{\varphi}_y(\varpi)) \end{pmatrix} \tag{133}$$

or in prograde/retrograde circular form (see Eq. 47), after some trigonometric manipulations.

4 Appendix 4: Matrices coefficients for the coupled model

$$\mathbf{K} = \begin{pmatrix} 0 & K_{1,2} & 0 & K_{1,4} & 0 & 0 & 0 & K_{1,8} & 0 & K_{1,10} \\ K_{2,1} & 0 & K_{2,3} & 0 & 0 & 0 & K_{2,7} & 0 & K_{2,9} & 0 \\ 0 & K_{3,2} & 0 & K_{3,4} & 0 & K_{3,6} & 0 & K_{3,8} & 0 & K_{3,10} \\ K_{4,1} & 0 & +K_{4,3} & 0 & K_{4,5} & 0 & K_{4,7} & 0 & K_{4,9} & 0 \\ 0 & 0 & 0 & K_{5,4} & 0 & K_{5,6} & 0 & K_{5,8} & 0 & K_{5,10} \\ 0 & 0 & K_{6,3} & 0 & K_{6,5} & 0 & K_{6,7} & 0 & K_{6,9} & 0 \\ 0 & n & 0 & 0 & 0 & 0 & 0 & -n & 0 & 0 \\ -n & 0 & 0 & 0 & 0 & 0 & n & 0 & 0 & 0 \\ 0 & 0 & 0 & 0 & 0 & n & 0 & 0 & 0 & -n \\ 0 & 0 & 0 & 0 & -n & 0 & 0 & 0 & n & 0 \end{pmatrix} \tag{134}$$

$$K_{1,2} = \frac{[(C_s - B_s)n + h_z(0)]}{A_s} \tag{135}$$

$$K_{1,4} = \frac{(C_{ot} - B_{ot})n}{A_s} \tag{136}$$

$$K_{1,8} = \frac{\kappa_{int}^x}{A_s} \tag{137}$$

$$K_{1,10} = -\frac{\kappa_{int}^x}{A_s} \tag{138}$$

$$K_{2,1} = \frac{[(A_s - C_s)n - h_z(0)]}{B_s} \tag{139}$$

$$K_{2,3} = \frac{(A_{ot} - C_{ot})n}{B_s} \tag{140}$$

$$K_{2,7} = \frac{3n(A_{s+ot} - C_{s+ot}) - \kappa_{int}^y}{B_s} \tag{141}$$

$$K_{2,9} = \frac{\kappa_{int}^y}{B_s} \tag{142}$$

$$K_{3,2} = n + \frac{(C_{ot} - A_{ot})n}{A_o} \tag{143}$$

$$K_{3,4} = -n - \frac{(C_o - A_o)n}{A_o} \tag{144}$$

$$K_{3,6} = K_{3,8} = -K_{3,10} = -\frac{(A_{ob} - C_{ob})n}{A_o} \tag{145}$$

$$K_{4,1} = -n - \frac{(C_{ot} - B_{ot})n}{B_o} \tag{146}$$

$$K_{4,3} = n + \frac{n(C_o - B_o)}{B_o} \tag{147}$$

$$K_{4,5} = K_{4,7} = -K_{4,9} = \frac{(B_{ob} - C_{ob})n}{B_o} \tag{148}$$

$$K_{5,4} = \frac{C_{ob} - B_{ob}}{A_i}n \tag{149}$$

$$K_{5,6} = \frac{(C_i - B_i)n}{A_i} \tag{150}$$

$$K_{5,8} = -K_{5,10} = -\frac{(C_{ob} - B_{ob})n + \kappa_{int}^x}{A_i} \tag{151}$$

$$K_{6,3} = \frac{(A_{ob} - C_{ob})n}{B_i} \tag{152}$$

$$K_{6,5} = \frac{(A_i - C_i)n}{B_i} \tag{153}$$

$$K_{6,7} = -\frac{(A_{ob} - C_{ob})n - \kappa_{int}^y}{B_i} \tag{154}$$

$$K_{6,9} = \frac{4(A_{ob} - C_{ob})n + 3(A_i - C_i)n - \kappa_{int}^y}{B_i} \tag{155}$$

For $\mathbf{K}_{ns}$, replace $K_{2,7}$ by $\frac{-\kappa_{int}^y}{B_s}$ and $K_{6,9}$ by $\frac{(A_{ob} - C_{ob})n - \kappa_{int}^y}{B_i}$.

5 Appendix 5: A precession model decoupled from the polar motion

We transform the angular momentum Eqs. (54–56) expressed in the coordinates of the shell and interior BF into three equations expressed in the coordinates of the IF attached to the Laplace plane (hence the mention (IF) in the subscripts below):

$$\frac{d\mathbf{H}_s}{dt} + \mathbf{\Omega}_s \wedge \mathbf{H}_s = \mathbf{\Gamma}_s \Rightarrow \frac{d\mathbf{H}_{s(IF)}}{dt} = \mathbf{\Gamma}_{s(IF)}, \tag{156}$$

$$\frac{d\mathbf{H}_{o(s)}}{dt} + \mathbf{\Omega}_s \wedge \mathbf{H}_{o(s)} = \mathbf{\Gamma}_{o(s)} \Rightarrow \frac{d\mathbf{H}_{o(IF)}}{dt} = \mathbf{\Gamma}_{o(IF)}, \tag{157}$$

$$\frac{d\mathbf{H}_i}{dt} + \mathbf{\Omega}_i \wedge \mathbf{H}_i = \mathbf{\Gamma}_i \Rightarrow \frac{d\mathbf{H}_{i(IF)}}{dt} = \mathbf{\Gamma}_{i(IF)}. \tag{158}$$

Note that we do not consider the periodic tidal deformations of the satellite and the effects of atmosphere and lakes here.

By analogy with the angular momentum of a solid satellite (Eq. A.13 of Baland et al. (2012)), the angular momentum of a layer k can simply be written as

$$\mathbf{H}_{k(IF)} = nC_k\hat{s}_k, \tag{159}$$

with $\hat{s}_k = (s_x^k, s_y^k, s_z^k \simeq 1)$ the unit vector along the rotation axis.

The torque $\mathbf{\Gamma}_{k(IF)}$ on layer k is the sum of the external torque by the parent planet and of the internal gravitational torque exerted by the other layers, both corrected for the effect of the hydrostatic pressure, and of the hydrodynamic pressure torque.

In the coordinates of the shell or interior BF, the expressions of the torque are given in Eqs. (109–111) and Eqs. (88–89). We transform them to the IF thanks to the following transformation matrices, defined by analogy with the transformation from a solid satellite BF to the IF (Eq. A.8 of Baland et al. (2012)):

$$R_{(s \to IF)} = R_z(-\xi_s).R_x(-\theta_s).R_z(-\phi_s), \tag{160}$$

$$R_{(i \to IF)} = R_z(-\xi_i).R_x(-\theta_i).R_z(-\phi_i). \tag{161}$$

Note that the polar motion and longitudinal librations of the solid layers are neglected in the matrices since we consider a decoupled model. As the precession is a slow motion, the torques are averaged over the orbit period, and we obtain

$$\mathbf{\Gamma}_{s(IF)} = n\kappa_s(\hat{s}_s \wedge \hat{n}) - nK(\hat{s}_s \wedge \hat{s}_i) + \mathbf{\Gamma}_{s(IF),\text{phd}}, \tag{162}$$

$$\mathbf{\Gamma}_{o(IF)} = \mathbf{\Gamma}_{o(IF),\text{phd}}, \tag{163}$$

$$\mathbf{\Gamma}_{i(IF)} = n\kappa_i(\hat{s}_i \wedge \hat{n}) + nK(\hat{s}_s \wedge \hat{s}_i) + \mathbf{\Gamma}_{i(IF),\text{phd}}, \tag{164}$$

with $\hat{n}$ defined as in Eq. (103). The coupling constants of the external and internal torques, $\kappa_{s/i}$ and K, respectively, are given by

$$\kappa_s = \frac{3}{2}n(C_s - A_s + C_{ot} - A_{ot}), \tag{165}$$

$$\kappa_i = \frac{3}{2}n(C_i - A_i + C_{ob} - A_{ob}), \tag{166}$$

$$K = -\frac{8\pi G}{5n}\left(\left(C_{i+ob} - \frac{A_{i+ob} + B_{i+ob}}{2}\right)(\rho_s(\alpha_s - \alpha_o) + \rho_o\alpha_o) \right.$$
$$\left. + \left(\frac{B_{i+ob} - A_{i+ob}}{4}\right)(\rho_s(\beta_s - \beta_o) + \rho_o\beta_o)\right), \tag{167}$$

(see also Baland et al. 2012, 2016 for the terms in $\kappa_{s,i}$ and K).

Expressions for the hydrodynamic pressure torques in the IF at the top and bottom of the liquid layer have been derived by Peale et al. (2014, 2016) for a biaxial planet (simply called *pressure torque* therein). Here we present a full demonstration for a triaxial satellite. As we have seen above, in the shell BF, the hydrodynamic torque on the shell $\mathbf{\Gamma}_{s,\text{phd}}$ reads as Eq. (88). We need to express this torque in the variables to be solved for in the decoupled model, which are ($s_x^s = \theta_s \cos(\xi_s - \pi/2)$, $s_y^s = \theta_s \sin(\xi_s - \pi/2)$, $s_x^o = \theta_o \cos(\xi_o - \pi/2)$, and $s_y^o = \theta_o \sin(\xi_o - \pi/2)$), instead of the variables (m_x^o, m_y^o) of the coupled model. This can be done by noting that in the shell BF, neglecting librations, the ocean rotation vector is given by (see Eq. 63)

$$\mathbf{\Omega}_{o(s)} = n\begin{pmatrix} m_x^o \\ m_y^o \\ 1 \end{pmatrix} \tag{168}$$

but can also be written by transforming the ocean rotation vector in the reference frame related to the rotation equator $(0, 0, n)$ to the BF of the shell:

$$\mathbf{\Omega}_{o(s)} = R_z[\phi_s].R_x[\theta_s].R_z[\xi_s - \xi_o].R_x[-\theta_o].\begin{pmatrix} 0 \\ 0 \\ n \end{pmatrix}, \tag{169}$$

with $\phi_s = -\xi_s + \Omega + \omega - \pi + M$, so that

$$m_x^o = \theta_o \sin(M + \omega - \xi_o + \Omega) - \theta_s \sin(M + \omega - \xi_s + \Omega), \tag{170}$$
$$m_y^o = \theta_o \cos(M + \omega - \xi_o + \Omega) - \theta_s \cos(M + \omega - \xi_s + \Omega). \tag{171}$$

We stress that, although we have neglected the polar motion $\mathbf{m}_s$ and $\mathbf{m}_i$ of the solid layers in order to obtain a decoupled precession model, we do not neglect the motion of the ocean rotation axis with respect to the shell BF $\mathbf{m}_o$, which is not an *ocean polar motion*, as it is defined with respect to the BF of the shell. We then express the torque in the IF thanks to the appropriate rotations:

$$\mathbf{\Gamma}_{s(IF),\mathrm{phd}} = R_{(s \to IF)}.\mathbf{\Gamma}_{s,\mathrm{phd}} \tag{172}$$

and average it over an orbit period with the slowly varying angles Ω, ξ_s and ξ_o held constant, to get

$$\mathbf{\Gamma}_{s(IF),\mathrm{phd}} = n\left(C_{ot} - \frac{A_{ot} + B_{ot}}{2}\right)(\hat{s}_s \wedge \hat{s}_o). \tag{173}$$

This torque has the same form as in the axially symmetric case, as $(A_{ot} + B_{ot})/2$ is the mean equatorial moment of inertia of the top ocean.

Similarly, it is possible to show that the hydrodynamic pressure torque on the interior, expressed in the IF and averaged over the orbit period, is given by

$$\mathbf{\Gamma}_{i(IF),\mathrm{phd}} = n\left(C_{ob} - \frac{A_{ob} + B_{ob}}{2}\right)(\hat{s}_i \wedge \hat{s}_o) \tag{174}$$

and that the corresponding torque on the ocean can be written as

$$\mathbf{\Gamma}_{o(IF),\mathrm{phd}} = -\mathbf{\Gamma}_{s(IF),\mathrm{phd}} - \mathbf{\Gamma}_{i(IF),\mathrm{phd}}. \tag{175}$$

Making use of Eqs. (162–164) and of Eqs. (173–175), the system of angular momentum equations (156–158) becomes

$$\dot{\mathbf{u}}_d + \mathbf{K_d}.\mathbf{u}_d = n\begin{pmatrix} \kappa_s N \\ 0 \\ \kappa_i N \end{pmatrix}, \tag{176}$$

with

$$\mathbf{u}_d = \begin{pmatrix} S_s \\ S_o \\ S_i \end{pmatrix}, \quad \mathbf{K_d} = \begin{pmatrix} \dfrac{K - \kappa_s - \kappa_{\mathrm{phd}}^s}{C_s} & \dfrac{\kappa_{\mathrm{phd}}^s}{C_s} & -\dfrac{K}{C_s} \\ \dfrac{\kappa_{\mathrm{phd}}^i}{C_o} & \dfrac{-\kappa_{\mathrm{phd}}^i - \kappa_{\mathrm{phd}}^s}{C_o} & \dfrac{\kappa_{\mathrm{phd}}^i}{C_o} \\ -\dfrac{K}{C_i} & \dfrac{\kappa_{\mathrm{phd}}^i}{C_i} & \dfrac{K - \kappa_i - \kappa_{\mathrm{phd}}^i}{C_i} \end{pmatrix}. \tag{177}$$

$\kappa_{\mathrm{phd}}^{s/i}$ are the coupling constants of the hydrodynamic pressure torques

$$\kappa_{\mathrm{phd}}^s = n\left(C_{ot} - \frac{A_{ot} + B_{ot}}{2}\right), \tag{178}$$

$$\kappa^i_{\text{phd}} = n\left(C_{ob} - \frac{A_{ob} + B_{ob}}{2}\right). \tag{179}$$

$S_j = s^j_x + I s^j_y$ and $N = n_x + I n_y$ are the projections onto the Laplace plane of the spin and orbit unit vectors, respectively.

For a uniformly precessing satellite, at first order in small orbital inclination i, the forcing is given by

$$N \simeq i\, e^{I(\Omega - \pi/2)}, \tag{180}$$

with Ω the longitude of the orbital ascending node. By substituting the projected spin vectors in the explicit form, correct up to the first order in i and in constant over time orbital obliquities η^j_0, of

$$S_j \simeq (i + \eta^j_0) e^{I(\Omega - \pi/2)} \tag{181}$$

into Eq. (176), we find that

$$\eta^j_0 = -\frac{i\,\dot{\Omega}\,n_j}{C_s C_o C_i (d_0 + d_1 \dot{\Omega} + d_2 \dot{\Omega}^2 + \dot{\Omega}^3)}, \tag{182}$$

with

$$n_s = \Big[C_s \left(\kappa^i_{\text{phd}} (\dot{\Omega}(C_i + C_o) + \kappa_i + \kappa^s_{\text{phd}}) + (C_i \dot{\Omega} + \kappa_i) \right.$$

$$(C_o \dot{\Omega} + \kappa^s_{\text{phd}}) - K(C_o \dot{\Omega} + \kappa^i_{\text{phd}} + \kappa^s_{\text{phd}}) \Big) \tag{183}$$

$$+ C_o \left(\kappa^s_{\text{phd}} (C_i \dot{\Omega} + \kappa_i + \kappa^i_{\text{phd}}) - K(\kappa^i_{\text{phd}} + \kappa^s_{\text{phd}}) \right) \tag{184}$$

$$- C_i \left(K(C_o \dot{\Omega} + \kappa^i_{\text{phd}} + \kappa^s_{\text{phd}}) - \kappa^i_{\text{phd}} \kappa^s_{\text{phd}} \right) \Big], \tag{185}$$

$$n_o = \Big[C_o \left((C_i \dot{\Omega} + \kappa_i + \kappa^i_{\text{phd}})(C_s \dot{\Omega} + \kappa_s + \kappa^s_{\text{phd}}) \right. \tag{186}$$

$$- K(\dot{\Omega}(C_i + C_s) + \kappa_i + \kappa^i_{\text{phd}} + \kappa_s + \kappa^s_{\text{phd}}) \Big) \tag{187}$$

$$+ C_i \left(C_s \dot{\Omega} (\kappa^i_{\text{phd}} + \kappa^s_{\text{phd}}) + \kappa^i_{\text{phd}}(\kappa_s + \kappa^s_{\text{phd}}) - K(\kappa^i_{\text{phd}} + \kappa^s_{\text{phd}}) \right) \tag{188}$$

$$+ C_s \left(\kappa^s_{\text{phd}}(\kappa_i + \kappa^i_{\text{phd}}) - K(\kappa^i_{\text{phd}} + \kappa^s_{\text{phd}}) \right) \Big], \tag{189}$$

$$n_i = \Big[C_i \left(\dot{\Omega}(C_o(\kappa_s + \kappa^s_{\text{phd}}) + C_s(\kappa^i_{\text{phd}} + \kappa^s_{\text{phd}})) + C_o C_s \dot{\Omega}^2 \right. \tag{190}$$

$$- K(C_o \dot{\Omega} + \kappa^i_{\text{phd}} + \kappa^s_{\text{phd}}) + \kappa^i_{\text{phd}} \kappa_s + \kappa^i_{\text{phd}} \kappa^s_{\text{phd}} + \kappa^i_{\text{phd}} + \kappa_s \kappa^s_{\text{phd}} \Big) \tag{191}$$

$$+ C_o \left(\kappa^i_{\text{phd}}(C_s \dot{\Omega} + \kappa_s + \kappa^s_{\text{phd}}) - K(\kappa^i_{\text{phd}} + \kappa^s_{\text{phd}}) \right) \tag{192}$$

$$- C_s \left(K(C_o \dot{\Omega} + \kappa^i_{\text{phd}} + \kappa^s_{\text{phd}}) - \kappa^i_{\text{phd}} \kappa^s_{\text{phd}} \right) \Big], \tag{193}$$

$$d_0 = \frac{\kappa_i \kappa^i_{\text{phd}} \kappa_s + \kappa_i \kappa^i_{\text{phd}} \kappa^s_{\text{phd}} + \kappa_i \kappa_s \kappa^s_{\text{phd}} + \kappa^i_{\text{phd}} \kappa_s \kappa^s_{\text{phd}}}{C_i C_o C_s} \tag{194}$$

$$+ \frac{-\kappa_i \kappa^i_{\text{phd}} K - \kappa_i \kappa^s_{\text{phd}} K - \kappa^i_{\text{phd}} \kappa_s K - \kappa_s \kappa^s_{\text{phd}} K}{C_i C_o C_s}, \tag{195}$$

$$d_1 = \frac{\kappa_i \kappa^i_{\text{phd}} + \kappa_i \kappa^s_{\text{phd}} + \kappa^i_{\text{phd}} \kappa^s_{\text{phd}} - \kappa^i_{\text{phd}} K - \kappa^s_{\text{phd}} K}{C_i C_o} \tag{196}$$

$$+ \frac{\kappa_i \kappa_s + \kappa_i \kappa_{\mathrm{phd}}^s + \kappa_{\mathrm{phd}}^i \kappa_s + \kappa_{\mathrm{phd}}^i \kappa_{\mathrm{phd}}^s}{C_i C_s} \tag{197}$$

$$+ \frac{-\kappa_i K - \kappa_{\mathrm{phd}}^i K - \kappa_s K - \kappa_{\mathrm{phd}}^s K}{C_i C_s} \tag{198}$$

$$+ \frac{\kappa_{\mathrm{phd}}^i \kappa_s + \kappa_{\mathrm{phd}}^i \kappa_{\mathrm{phd}}^s + \kappa_s \kappa_{\mathrm{phd}}^s - \kappa_{\mathrm{phd}}^i K - \kappa_{\mathrm{phd}}^s K}{C_o C_s}, \tag{199}$$

$$d_2 = \frac{\kappa_i + \kappa_{\mathrm{phd}}^i - K}{C_i} + \frac{\kappa_{\mathrm{phd}}^i + \kappa_{\mathrm{phd}}^s}{C_o} + \frac{\kappa_s + \kappa_{\mathrm{phd}}^s - K}{C_s}. \tag{200}$$

By analogy with the constant over time obliquity η_0 from Eq. (44) for the solid case, we use the subscript 0 to indicate that the quantities η_0^j correspond to the solution of a precession model decoupled from the polar motion of the solid layers.

References

Araki, H., Tazawa, S., Noda, H., Ishihara, Y., Goossens, S., Sasaki, S., Kawano, N., Kamiya, I., Otake, H., Oberst, J., Shum, C.: Lunar global shape and polar topography derived from Kaguya-LALT laser altimetry. Science **323**, 897 (2009). https://doi.org/10.1126/science.1164146

Baland, R.M., Van Hoolst, T., Yseboodt, M., Karatekin, Ö.: Titan's obliquity as evidence of a subsurface ocean? Astron. Astrophys. **530**, A141 (2011). https://doi.org/10.1051/0004-6361/201116578

Baland, R.M., Yseboodt, M., Van Hoolst, T.: Obliquity of the Galilean satellites: the influence of a global internal liquid layer. Icarus **220**, 435 (2012). https://doi.org/10.1016/j.icarus.2012.05.020

Baland, R.M., Tobie, G., Lefèvre, A., Van Hoolst, T.: Titan's internal structure inferred from its gravity field, shape, and rotation state. Icarus **237**, 29 (2014). https://doi.org/10.1016/j.icarus.2014.04.007

Baland, R.M., Yseboodt, M., Van Hoolst, T.: The obliquity of Enceladus. Icarus **268**, 12 (2016). https://doi.org/10.1016/j.icarus.2015.11.039

Bills, B.G.: Free and forced obliquities of the Galilean satellites of Jupiter. Icarus **175**, 233 (2005). https://doi.org/10.1016/j.icarus.2004.10.028

Bills, B.G., Nimmo, F.: Free and forced obliquities of the Galilean satellites of Jupiter. Icarus **196**, 293 (2008). https://doi.org/10.1016/j.icarus.2008.03.002

Boué, G., Rambaux, N., Richard, A.: Rotation of a rigid satellite with a fluid component: a new light onto Titan's obliquity. Celest. Mech. Dyn. Astron. **129**, 449 (2017). https://doi.org/10.1007/s10569-017-9790-8

Colombo, G.: Cassini's second and third laws. Astron. J. **71**, 891 (1966). https://doi.org/10.1086/109983

Coyette, A., Van Hoolst, T., Baland, R.M., Tokano, T.: Modeling the polar motion of Titan. Icarus **265**, 1 (2016). https://doi.org/10.1016/j.icarus.2015.10.015

Coyette, A., Baland, R.M., Van Hoolst, T.: Variations in rotation rate and polar motion of a non-hydrostatic Titan. Icarus **307**, 83 (2018). https://doi.org/10.1016/j.icarus.2018.02.003

Defraigne, P., Dehant, V., Pâquet, P.: Link between the retrograde-prograde nutations and nutations in obliquity and longitude. Celest. Mech. Dyn. Astron. **62**, 363 (1995). https://doi.org/10.1007/BF00692286

Dehant, V., Mathews, P.M.: Precession, Nutation and Wobble of the Earth (2015)

Dumberry, M., Wieczorek, M.A.: The forced precession of the Moon's inner core. J. Geophys. Res. (Planets) **121**, 1264 (2016). https://doi.org/10.1002/2015JE004986

Eckhardt, D.H.: Theory of the libration of the moon. Moon Planets **25**, 3 (1981). https://doi.org/10.1007/BF00911807

Margot, J.L., Peale, S.J., Jurgens, R.F., Slade, M.A., Holin, I.V.: Effect of core-mantle and tidal torques on Mercury's spin axis orientation. Science **316**, 710 (2007)

Margot, J.L., Peale, S.J., Solomon, S.C., Hauck II, S.A., Ghigo, F.D., Jurgens, R.F., Yseboodt, M., Giorgini, J.D., Padovan, S., Campbell, D.B.: Mercury's moment of inertia from spin and gravity data. J. Geophys. Res. (Planets) **117**, E00L09 (2012). https://doi.org/10.1029/2012JE004161

Mathews, P.M., Buffett, B.A., Herring, T.A., Shapiro, I.I.: Forced nutations of the earth: influence of inner core dynamics. I—Theory. II—Numerical results and comparisons. III - Very long interferometry data analysis. J. Geophys. Res. **96**, 8219 (1991). https://doi.org/10.1029/90JB01955

Meriggiola, R., Iess, L., Stiles, B.W., Lunine, J.I., Mitri, G.: The rotational dynamics of Titan from Cassini RADAR images. Icarus **275**, 183 (2016). https://doi.org/10.1016/j.icarus.2016.01.019

Moritz, H., Mueller, I.I.: Earth rotation : theory and observation (1987)

Noyelles, B., Nimmo, F.: On the time-variable nature of Titan's obliquity. In: AAS/Division of Dynamical Astronomy Meeting, vol. 45, p. 301.03 (2014)

Noyelles, B.: Behavior of nearby synchronous rotations of a Poincaré–Hough satellite at low eccentricity. Celest. Mech. Dyn. Astron. **112**, 353 (2012). https://doi.org/10.1007/s10569-012-9398-y

Noyelles, B.: Rotation of a synchronous viscoelastic shell. Mon. Not. R. Astron. Soc. **474**, 5614 (2018). https://doi.org/10.1093/mnras/stx3122

Peale, S.J.: Generalized Cassini's laws. Astron. J. **74**, 483 (1969). https://doi.org/10.1086/110825

Peale, S.J., Margot, J.L., Hauck, S.A., Solomon, S.C.: Effect of core-mantle and tidal torques on Mercury's spin axis orientation. Icarus **231**, 206 (2014). https://doi.org/10.1016/j.icarus.2013.12.007

Peale, S.J., Margot, J.L., Hauck, S.A., Solomon, S.C.: Consequences of a solid inner core on Mercury's spin configuration. Icarus **264**, 443 (2016). https://doi.org/10.1016/j.icarus.2015.09.024

Rambaux, N., Williams, J.G.: The Moon's physical librations and determination of their free modes. Celest. Mech. Dyn. Astron. **109**, 85 (2011). https://doi.org/10.1007/s10569-010-9314-2

Sasao, T., Okubo, S., Saito, M.: A Simple theory on dynamical effects of stratified fluid core upon nutational motion of the Earth. In: Duncombe, R.L. (Ed.) Nutation and the Earth's Rotation, IAU Symposium, vol. 78, p. 165 (1980)

Smith, M.L.: Wobble and nutation of the earth. Geophys. J. **50**, 103 (1977). https://doi.org/10.1111/j.1365-246X.1977.tb01326.x

Tokano, T.: Wind-induced equatorial bulge in Venus and Titan general circulation models: implication for the simulation of superrotation. Geophys. Res. Lett. **40**, 4538 (2013). https://doi.org/10.1002/grl.50841

Tokano, T., Lorenz, R.D.: Wind-driven circulation in Titan's seas. J. Geophys. Res. (Planets) **120**, 20 (2015). https://doi.org/10.1002/2014JE004751

Tokano, T., Lorenz, R.D., Van Hoolst, T.: Numerical simulation of tides and oceanic angular momentum of Titan's hydrocarbon seas. Icarus **242**, 188 (2014). https://doi.org/10.1016/j.icarus.2014.08.021

Van Hoolst, T.: The rotation of the terrestrial planets. Treatise Geochem. **10**, 123 (2007)

Van Hoolst, T., Dehant, V.: Influence of triaxiality and second-order terms in flattenings on the rotation of terrestrial planets. I. Formalism and rotational normal modes. Phys. Earth Planet. Inter. **134**, 17 (2002). https://doi.org/10.1016/S0031-9201(02)00068-7

Van Hoolst, T., Rambaux, N., Karatekin, Ö., Baland, R.M.: The effect of gravitational and pressure torques on Titan's length-of-day variations. Icarus **200**, 256 (2009). https://doi.org/10.1029/2009GL041465

Van Hoolst, T., Baland, R.M., Trinh, A.: On the librations and tides of large icy satellites. Icarus **226**, 299 (2013). https://doi.org/10.1016/j.icarus.2013.05.036

Varadi, F., Musotto, S., Moore, W., Schubert, G.: Normal modes of synchronous rotation. Icarus **176**, 235 (2005). https://doi.org/10.1016/j.icarus.2005.01.002

Vienne, A., Duriez, L.: TASS1.6: Ephemerides of the major Saturnian satellites. Astron. Astrophys. **297**, 588 (1995)

Williams, J.G., Boggs, D.H., Yoder, C.F., Ratcliff, J.T., Dickey, J.O.: Lunar rotational dissipation in solid body and molten core. J. Geophys. Res. **106**, 27933 (2001). https://doi.org/10.1029/2000JE001396

Zebker, H.A., Stiles, B., Hensley, S., Lorenz, R., Kirk, R.L., Lunine, J.: Size and shape of Saturn's Moon Titan. Science **324**, 921 (2009). https://doi.org/10.1126/science.1168905